Thymus-derived leukemia-lymphoma in mice transgenic for the Tax gene of human T-lymphotropic virus type I

Hideki Hasegawa[1,2,8], Hirofumi Sawa[3,4,8], Martha J Lewis[2,5], Yasuko Orba[3], Noreen Sheehy[2], Yoshie Yamamoto[6], Takeshi Ichinohe[1], Yasuko Tsunetsugu-Yokota[7], Harutaka Katano[1], Hidehiro Takahashi[1], Junichiro Matsuda[6], Tetsutaro Sata[1], Takeshi Kurata[1], Kazuo Nagashima[3] & William W Hall[2]

Adult T-cell leukemia-lymphoma (ATLL) is a group of T-cell malignancies caused by infection with human T-lymphotropic virus type I (HTLV-I). Although the pathogenesis of ATLL remains incompletely understood, the viral regulatory protein Tax is centrally involved in cellular transformation. Here we describe the generation of HTLV-I Tax transgenic mice using the Lck proximal promoter to restrict transgene expression to developing thymocytes. After prolonged latency periods, transgenic mice developed diffuse large-cell lymphomas and leukemia with clinical, pathological and immunological features characteristic of acute ATLL. Transgenic mice were functionally immunocompromised and they developed opportunistic infections. Fulminant disease also developed rapidly in SCID mice after engraftment of lymphomatous cells from transgenic mice. Flow cytometry showed that the cells were CD4⁻ and CD8⁻, but CD44⁺, CD25⁺ and cytoplasmic CD3⁺. This phenotype is indicative of a thymus-derived pre–T-cell phenotype, and disease development was associated with the constitutive activation of NF-κB. Our model accurately reproduces human disease and will provide a tool for analysis of the molecular events in transformation and for the development of new therapeutics.

HTLV-I infection is endemic in a number of well-defined geographical regions and it is estimated that as many as 20 million individuals are infected worldwide[1]. Although the vast majority of infected individuals remain clinically asymptomatic, some 2–5% will develop ATLL, which is a group of mature T-cell malignancies with distinct clinical presentations[2]. ATLL generally occurs in individuals infected around the time of birth and presents after prolonged latency periods ranging from 20 to 60 years. This is consistent with an age-dependent accumulation of leukemogenic events[1]. Transformed cells in ATLL are generally CD4⁺ T lymphocytes[2], although other, less common

phenotypes have been observed. These include CD4⁻CD8⁻ (refs. 3–7), CD8⁺ (ref. 8) and CD4⁺CD8⁺ transformed cells[9,10], which suggests that infection and transformation of distinct cell populations during thymic development is important in the pathogenesis of ATLL.

The distinct clinical subtypes of ATLL include the two indolent forms, smoldering and chronic, and the extremely aggressive forms, acute and lymphomatous[2,11]. Individuals with aggressive ATLL present with extensive lymphadenopathy, hepatosplenomegaly, visceral invasion and characteristic cutaneous infiltration by malignant cells. Acute ATLL is also characterized by an aggressive high-grade T-cell leukemia, with leukemic cells showing a characteristic morphology of abnormally enlarged and cleaved nuclei, which are termed 'flower cells.' In addition to being poorly responsive to treatment, individuals with ATLL are functionally immunocompromised and develop a range of opportunistic infections similar to those seen in individuals with AIDS, such as Pneumocystis jiroveci pneumonia[2,11].

Although the pathogenesis of ATLL remains incompletely understood, the viral regulatory protein Tax seems to have a central role[1,12,13]. Tax, an extremely pleiotropic protein, has been shown to transform primary lymphocytes. This transformation is related to the ability of Tax to dysregulate the transcription of genes involved in cellular proliferation, cell-cycle control and apoptosis. Tax is a potent transcriptional transactivator not only of viral but also of cellular gene expression. The protein physically interacts with a number of cellular transcription factors, which include components of the NF-κB–Rel signaling complex, and persistent and constitutive activation of NF-κB is central to the development and maintenance of the malignant phenotype in ATLL[12–14]. Activation of NF-κB by Tax results in upregulation of the expression of a large number of cellular genes involved in cell proliferation, including a number of cytokines and their corresponding receptor genes[1,12–15] and this is believed to contribute to the autonomous expansion of infected and transformed cell populations.
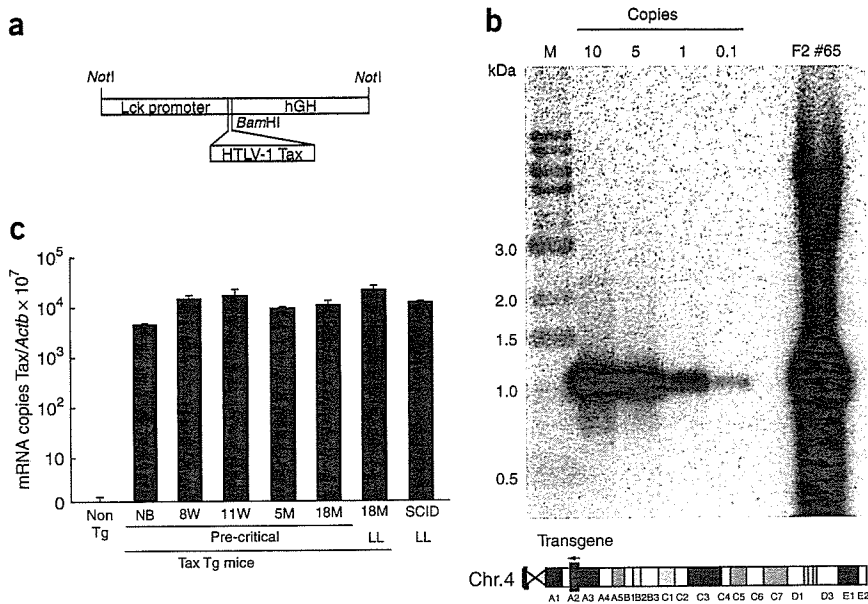
Figure 1 Construction of the Tax transgene and Tax mRNA expression in transgenic mice. (a) Schematic representation of the Tax transgene. HTLV-1 Tax cDNA was inserted in the BamHI site of the p1017 vector at the 3′ end of the Lck proximal promoter. (b) Estimation of integrated Tax copy number and mapping of the Tax integration site (transgenic mouse #65) by chromosomal walking analysis. Tax copy numbers were investigated by Southern blot analysis of BamHI-digested genomic DNA from the transgenic mouse (#65) in parallel with a serially diluted plasmid containing HTLV-I Tax cDNA. (c) Expression of Tax mRNA in Tax transgenic mice and SCID mice. RT-PCR was carried out on mRNAs extracted from spleens of newborn mice (NB), transgenic mice (Tg) at 8 weeks (8w), 11 weeks (11w), 5 months (5m), 18 months (18m), all without disease; 18 months with leukemia-lymphoma (18m LL) and in SCID mice with fulminant disease (SCID LL).

Attempts to directly show the oncogenic potential of Tax *in vivo* have been for the most part restricted to studies on expression of Tax in transgenic mouse models. These studies have resulted in a wide range of phenotypes, which have included the development of arthropathies, exocrinopathies, mesenchymal tumors, neurofibromas and large granular lymphocytic leukemia, a malignancy of natural killer cells[16–21]. None of the models, however, has developed T-cell lymphoma or leukemia identical to ATLL. To address this discrepancy, we have generated transgenic mice with expression of Tax restricted to devel-oping thymocytes, and we have shown that after prolonged latency periods these mice develop lymphoma and leukemia with the clinical, pathological and immunological features characteristic of human disease.

RESULTS

Lymphoma and leukemia in HTLV-1 Tax transgenic mice

We generated transgenic mice expressing Tax under the control of the Lck proximal promoter, which restricts expression to developing thymocytes[22,23] because infection and trans-formation of cells during thymic development seems to be important in the pathogenesis of the disorder (**Fig. 1a**). We obtained three founder mice for each of the three lineages (#53, #14 and #17) and although each of the lineages was cross-bred with transgene-negative littermates, offspring were obtained from only one founder (#53; **Table 1**). PCR and Southern blot analysis of all founders and the progeny mice confirmed that all progeny carried the transgene. We studied transgene copy numbers and integration sites in selected mice. This number ranged from 10 to >20 copies, and genome walking analysis showed that the transgenes were tandemly inserted and integrated in the A2 region at position 14783143 of chromosome 4, which is a none-ncoding region (**Fig. 1b**).

Gross pathological examination of Tax founder mice #14 and #17 killed at 23 months, and of all selected offspring from founder #53 ($n = 9$) beginning at 10 months, showed the development of marked spleno-megaly, hepatomegaly, lymphadenopathy and the presence of large mesenteric tumors (**Fig. 2a,b** and **Table 1**). Hepatosplenomegaly was characteristically a 5–20-fold increase in organ size (**Fig. 2a–c**). Lymphadenopathy

Table 1 Establishment of HTLV-I Tax transgenic mice

Founder	F1	F2	Gender	Killed (month)	Involvement	Leukemia
#53	#50		M	12	Liver, spleen, bone marrow	+
	#52		M	17	Liver, spleen, kidney, lymph nodes, lung, skin, bone marrow, thymus	+
		#11	M	11	Early killing	–
		#12	F	14 (dead)	Liver, spleen, kidney, lymph nodes, lung, skin	ND
		#20	F	12 (dead)	Thymus[a]	ND
		#22	F	10	Liver, spleen, kidney, lymph nodes, lung, skin, eyelid, meninges, bone marrow	+
		#33	M	10	Early killing	–
		#36	F	18	Liver, spleen, lymph nodes, lung, bone marrow, thymus	–
		#44	F	19 (dead)	Liver, spleen, lymph nodes, lung	ND
		#52	F	17	Early killing	–
		#65	M	8	Early killing	–
#14			M	23	Liver, spleen, kidney, lymph nodes, lung, skin	+
#17			F	23	Liver, spleen, kidney, lymph nodes, lung, skin	+

Offspring were generated from one of three founder mice (#53). Three mice (#11, #52, #65) were killed before the development of disease (early death). One mouse (#20) unexpectedly died. The remaining mice were killed at the time points indicated. Gross lymphomatous involvement was as noted and all tissues were subjected to histological examination. Peripheral blood smears were examined for leukemic cells using Giemsa staining. M, male; F, female; ND, not determined.
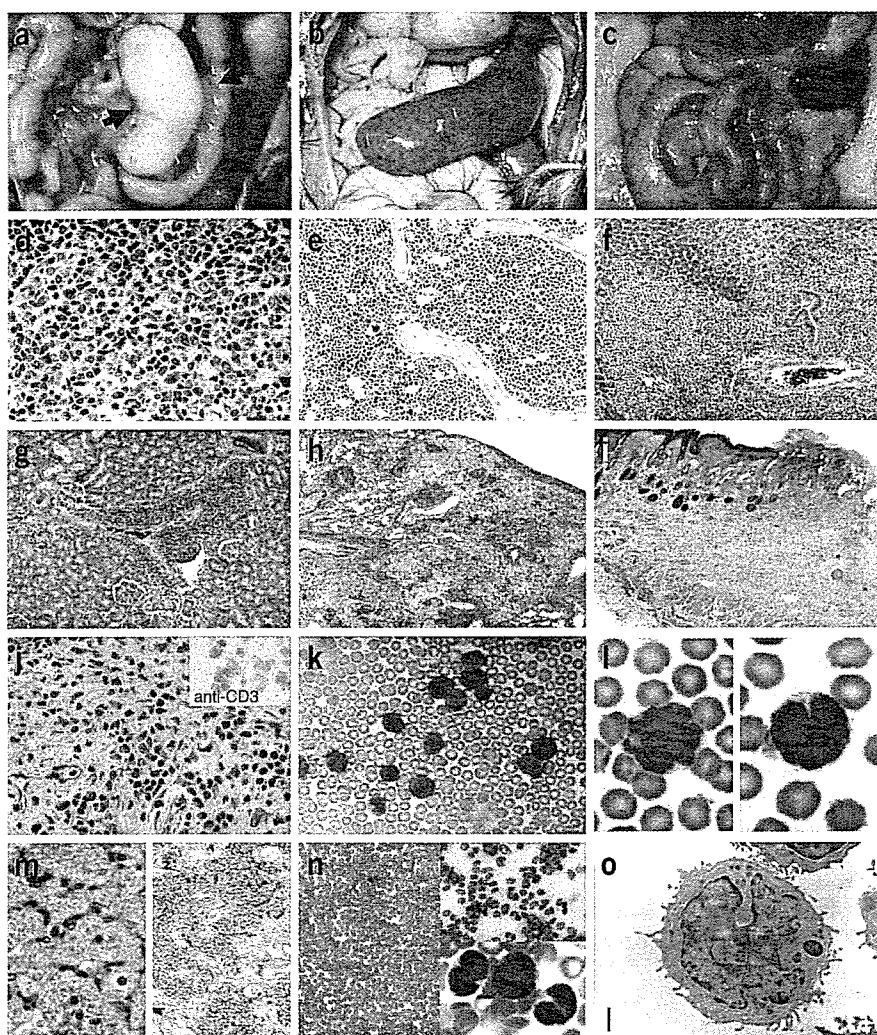[a]Thymus was exclusively examined; other organs were not examined.

Figure 2 Pathological findings of T-cell lymphoma and leukemia in Tax transgenic mice. (a) Mesenteric tumor (black arrows) in the abdominal cavity of transgenic mouse #52. (b) Marked splenomegaly in transgenic mouse #22 with a greater than fivefold increase in size compared to an age-matched control littermate. (c) No tumors, lymphadenopathy or splenomegaly were evident in the control mice. Histological findings using H&E staining showed diffuse large-cell lymphoma in mesenteric lymph node (d), bone marrow with complete replacement of the marrow by lymphomatous cells (e), liver (f), kidney (g), lung (h) and lymphomatous infiltration of the skin with associated ulceration (i). (j) H&E staining and immunohistochemical staining with positive CD3-specific antibody staining (insert) of lymphomatous cells in the skin. (k,l) Peripheral blood smears from transgenic mouse #22. Leukemic cells with large and cleaved nuclei morphologically identical to flower cells found in human disease were present in peripheral blood smears of five mice. (m) H&E and Grocott staining of the lung showing opportunistic infection with *P. jiroveci*. (n) Peripheral blood smear with a large number of leukemia cells with segmented nuclei in a SCID mouse at 28 d after intraperitoneal injection of splenic lymphomatous cells from a transgenic mouse (lower magnification, left upper panel; higher magnification, left lower panel). Blood smear of a control age-matched SCID mouse is shown in the left panel. (o) Electron microscopic examination of leukemic cells from ascites fluid of SCID mice (original magnification, ×6,000). Cells showed enlarged cerebriform nuclei with disrupted chromatin and scanty cytoplasms typical of human ATLL cells. Scale bar, 500 nm.

was most often observed in the mesenteric, cervical and axillary lymph nodes but, in several cases, inguinal nodes were also involved. The mesenteric tumors ranged in size from 0.5 to 2.5 cm. All nine transgenic mice examined developed pathology beginning at 10 months of age, and findings were evenly distributed between males and females (Table 1). Histological examination showed diffuse, large-cell lymphomas involving spleen, lymph nodes, liver, thymus, bone marrow, kidney, lung, meninges and skin (Fig. 2 and Table 1). Specifically, perivascular infiltration of lymphomatous cells was readily observed in the liver, kidney and lungs (Fig. 2f–h) and in mice with liver involvement; it seems likely that the cells had spread from the mesentery to the liver through the portal vein (Fig. 2f). Four mice examined had bone marrow involvement (Fig. 2e) with complete replacement of the marrow by lymphomatous cells. We documented involvement of the meninges in one mouse, but there was no evidence of invasion of the central nervous system parenchyma. Five of seven mice had cutaneous involvement with gross ulceration of the skin, and histologically had prominent infiltration of leukemic cells into the dermis, which is characteristic of ATLL. Immunohistochemical staining indicated that these cells expressed CD3 but not B220, showing that they were T-cell lymphomas (Fig. 2j). Overall, the histopathological findings are identical to those observed in ATLL, and the cytological characteristics of the lymphomatous cells are consistent with an aggressive

malignancy and with the myriad of chromosomal abnormalities found in the disease[13].

Giemsa staining of peripheral blood smears in five mice showed the presence of large and abnormal leukemic cells with cleaved nuclei, which were morphologically identical to the flower cells observed in ATLL (Fig. 2k,l).

We also examined age- and sex-matched transgene-negative littermates in parallel for each mouse. We did not detect lymphoma in any of the nontransgenic littermates; however, two littermates that died from unknown causes did not have any abnormal gross or microscopic pathology. Three mice were killed before the development of disease, but there was no evidence of leukemia or lymphoma (Table 1). In addition to the development of leukemia and lymphoma, we found that transgenic mice were clinically immunocompromised. Mice with disease, but not control mice housed under identical conditions, developed severe pulmonary infections with *P. jiroveci* (Fig. 2m), which is characteristic of human ATLL.

Transfer of leukemia and lymphoma to immunodeficient mice

To develop a more consistent and rapid model of disease development and to facilitate immunological analyses, we attempted to induce leukemia and lymphoma in mice with severe combined immun-deficiency (SCID) after intraperitoneal and intradermal injection of lymphomatous spleen cells from individual transgenic mice. After
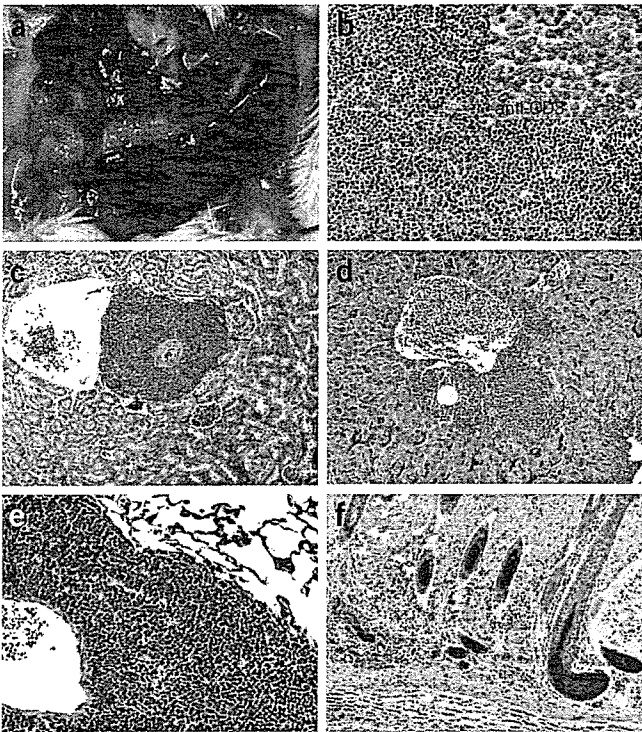
Figure 3 Gross and histological findings of lymphoma in SCID mice at 28 d after intradermal injection of lymphomatous cells from Tax transgenic mice. (a) Gross splenomegaly. Histological findings in spleen (b; insert, immunostaining showing positive staining for CD3-specific antibody), liver (c), kidney (d), lung (e) and skin (f). All organs showed extensive lymphomatous invasion.

direct transfer of cells from three transgenic mice, all SCID mice died within 28 d, having developed both an extremely aggressive leukemia with characteristic flower cells (Fig. 2m) and extensive lymphomatous involvement of the spleen, lymph nodes, bone marrow, liver, kidney and lung, which was identical to that observed in the original transgenic mice (Fig. 3). Notably, cutaneous involvement was only observed in those mice into which cells had been transferred by intradermal injection. Transmission electron microscopy of leukemic cells recovered from ascites fluid from SCID mice showed grossly enlarged and segmented cerebriform nuclei with markedly thin and scanty cytoplasms and a loss of polarity similar to that reported for ATLL and Sezary syndrome (Fig. 2o).

Flow cytometry analysis

We used flow cytometry to characterize the cell populations in both transgenic and SCID mice. Cells from transgenic spleens showed marked size heterogeneity with considerably higher forward scatter and side scatter compared to cells derived from spleens of control mice (Fig. 4a). Immunostaining of cells from SCID mice showed these were a distinct population and had a CD3$^-$CD4$^-$CD8$^-$CD34$^-$c-kit$^-$ phenotype (Fig. 4b,c). Staining for B-cell markers (B220) and macrophage markers (Mac 1) was negative (data not shown). Further analysis of SCID mice showed that the cells were CD44$^+$CD25$^+$ (Fig. 4c) and positive for cytoplasmic but not surface CD3 in both flow cytometric and immunofluorescence studies (Fig. 4d,e), all of which is consistent with a pre–T-cell, double-negative phenotype (Fig. 4f). A characteristic feature of ATLL is overexpression of CD25 (also known as IL-2 receptor α) on the surface of the transformed cells, and it is believed that Tax-mediated upregulation of both interleukin (IL)-2 and the IL-2 receptor has a major role in the autonomous proliferation of the transformed cell populations[14]. We examined the expression of CD25 in splenic lymphoma cells, and although the expression levels varied between tumor cells from different mice, a marked increase in expression was always evident (Fig. 4d). In addition, the T-cell

activation marker CD69 was also found to be expressed at high levels on the lymphomatous cells (Fig. 4d).

NF-κB activation in transgenic and SCID mice

As it is well established that activation of NF-κB by Tax has a crucial role in transformation of cells by HTLV-I and in the maintenance of the malignant phenotype[12–14], we examined activity of NF–κB using both electrophoretic mobility shift assays (EMSAs) and enzyme-linked immunosorbent assays (ELISAs). EMSAs on nuclear extracts from transgenic splenic lymphoma cells showed marked NF-κB activity (Fig. 5) similar to that in a Epstein-Barr virus–transformed lymphoblastoid cell line used as a positive control. In contrast, no activity was evident in cells from normal mice (Fig. 5a). In addition, supershift assays (Fig. 5b) showed supershifted bands in the presence of antibodies for p50 and c-Rel, suggesting that formation of the p50–c-Rel complex is involved in the development and maintenance of the malignant phenotype (Fig. 5b). Evaluation of lymphomatous cells from SCID mice also confirmed activation of NF-κB. In contrast to the case of transgenic mice, this activation was found to involve only c-rel (Supplementary Fig. 1 online). We also examined SCID mice by ELISA for activation of CREB, which was shown to be absent (Supplementary Fig. 1 online).

Expression of Tax in transgenic mice

We used RT-PCR analysis of RNAs from splenic tissues to determine whether development of disease in both transgenic and SCID mice was associated with active expression of Tax (Fig. 1c). Although expression levels were low (10^4 less than expression of Ac-tb, which encodes β-actin), Tax mRNA could be readily detected in newborn, asymptomatic, early-killed mice and in both transgenic and SCID mice with overt disease.

DISCUSSION

Here we showed that Tax expression alone in transgenic mice is sufficient to initiate the development of T-cell lymphoma and leukemia with clinical, pathological and immunological features similar or identical to those observed in ATLL. Specifically, the disorder in mice occurs after prolonged latency periods ranging from 10 to 23 months, which would be equivalent to the 20–60 years observed in human disease. The long time period before the onset of disease in the transgenic mouse model is also consistent with a multistep process of transformation. The clinical and pathological features of the disease were identical to those observed in the aggressive forms of ATLL, with widespread organ invasion by lymphomatous cells and the development of leukemia. Notably, the leukemia displayed the typical appearance of flower cells characteristic of ATLL, and these cells also had the expected morphological features when examined by electron microscopy.

ATLL has prominent cutaneous involvement, and this was reproduced in the transgenic model. Transgenic mice were also clinically immunocompromised and developed pulmonary infections with P. jiroveci, which is also characteristic of ATLL. The development of disease in transgenic mice and after transfer of disease to SCID mice was associated with activation of NF-κB, which is also found in ATLL.
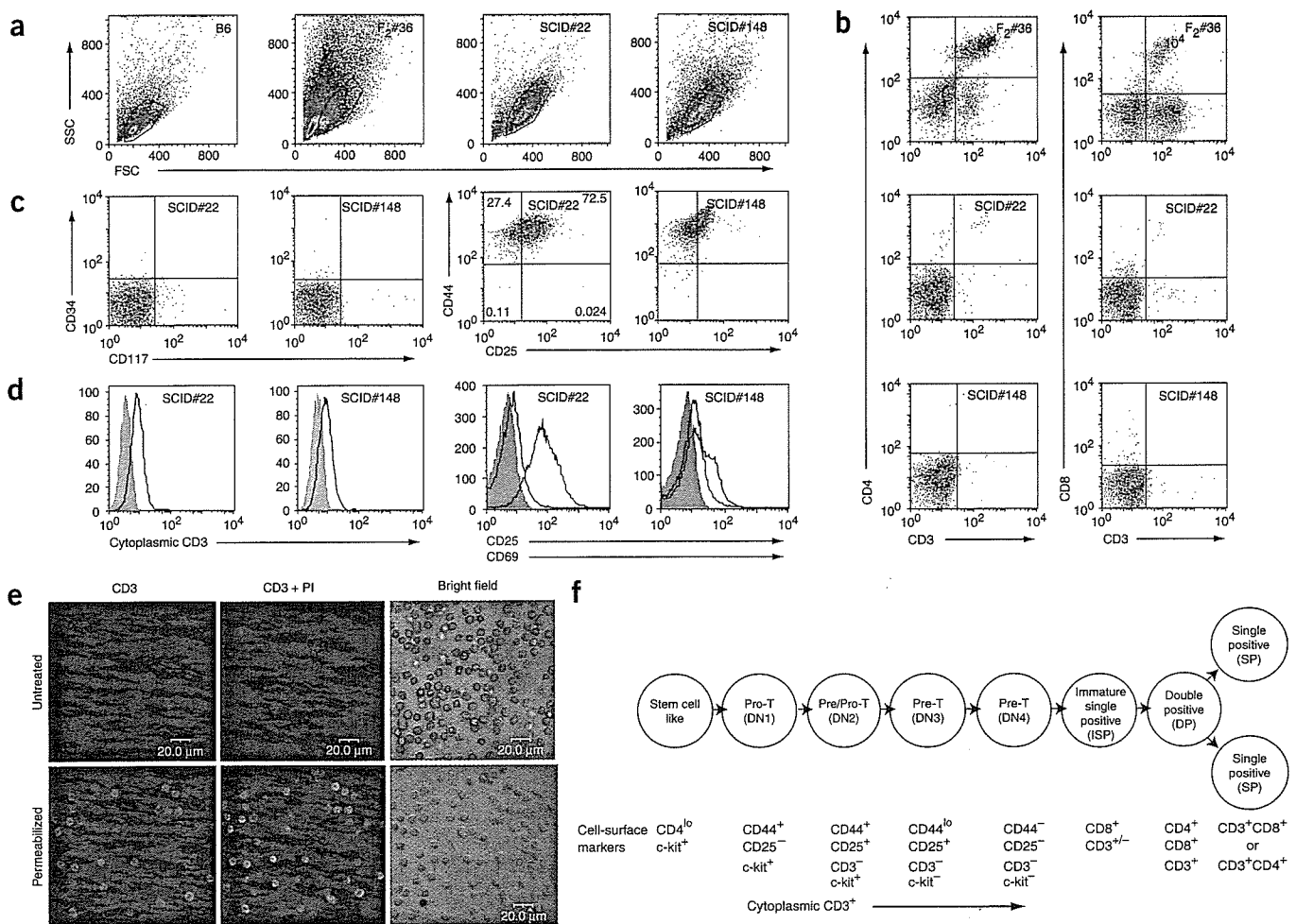
Figure 4 Flow cytometry analysis of cell-surface and intracellular markers in lymphomatous cells. We analyzed spleen-cell suspensions from transgenic mice with leukemia-lymphoma (#36), littermate control mouse (B6) and two SCID mice (#22, #148) with overt disease. (a) Forward-scatter (FSC) and side-scatter (SSC) analysis. (b) Expression of cell-surface markers CD3, CD4 and CD8. (c) Expression of cell-surface markers CD34, CD117 (also known as c-kit), CD44 and CD25. (d) Expression of CD25, CD69 and cytoplasmic CD3. (e) Surface and cytoplasmic CD3 staining of lymphomatous cells from SCID mice (SCID #22) with fulminant disease. Immunofluorescence studies show an absence of CD3 surface staining (untreated) but consistent and uniform cytoplasmic staining in permeabilized cells. Staining of nuclei using propidium iodide (PI) is indicated. (f) Schematic representation of T-cell development and corresponding immunological markers in the mouse thymus.

In the transgenic mice, this involved both the p50 and c-rel components, whereas after transfer to SCID mice, only c-rel seemed to be involved. The reasons for this are unclear, but such differences have also been observed in individuals with ATLL[24].

The malignant phenotype observed in the transgenic mice was a CD4⁻CD8⁻ double negative. Flow cytometric analysis also showed that transformed cells were CD44+ and c-kit⁻. Although surface staining for CD3 was negative, cytoplasmic CD3 staining was readily shown, and overall the cell markers were consistent with a thymic pre–T-cell phenotype[25,26]. The most common presenting phenotype in ATLL is CD4+; however, there have been numerous reports describing the CD4⁻CD8⁻ phenotype in a considerable number of individuals with ATLL[3–7]. The different phenotypes observed in ATLL may well reflect the temporal relationships between infection with expression of Tax and the cell populations present at different stages of thymic development. It is likely that infection in most cases of human disease occurs after birth and much later than in our model. We are currently exploring the possibility of modifying the Lck promoters to allow control of Tax expression at different stages of thymic development to

assess whether this will result in different phenotypes. It seems highly probable that use of the Lck promoter, which restricts expression of the transgene to developing thymocytes, has been crucial to the success of our mouse model. As noted previously, ATLL occurs after vertical transmission and is specifically associated with a history of breastfeeding. In rat models, intravenous or intraperitoneal inoculation of HTLV-I–infected cell lines results in considerable humoral and cellular immune responses. In contrast, these are absent after oral inoculation, and this hyporesponsiveness seems to contribute to successful infection[27]. Thus, both oral tolerance and the tropism of the virus for infection of developing T lymphocytes seem to be two key factors in the development of ATLL.

One major difference between our model and human disease is expression of Tax. Expression of Tax is rarely detected in ATLL, and this circumstance is thought to result primarily from highly efficient Tax-specific cellular immune responses that can effectively eliminate Tax-expressing T lymphocytes. Such responses, however, would certainly not occur in either transgenic or SCID mice. It has also been suggested that the lack of Tax expression in ATLL may be the result of
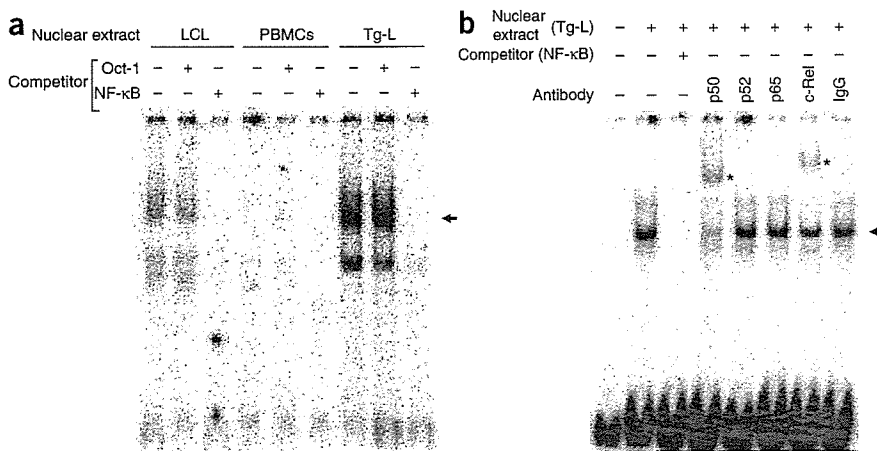
DNA libraries of the transgenic mice using tail-tip DNA digested with four restriction enzymes: DraI, PvuII, EcoRV and StuI; the genomic walk consisted of two PCR amplifications. We determined nucleotide sequences of PCR products by direct sequencing and identified specific chromosomal transgene insertion sites using BLAST searches of the flanking sequences in the Ensembl genome database.

Histopathological examination and immunohistochemistry. We directly fixed tissues in neutral-buffered formalin (Sigma), embedded them in paraffin, and sectioned and stained them with H&E. We stained additional sections with Grocott staining for detection of *P. jiroveci* cysts. We stained skin sections with CD3-specific antibody (Santa Cruz Biotechnology). We prepared peripheral blood smears using Giemsa staining and examined them with light microscopy.

Figure 5 EMSAs showing activation of NF-κB in lymphomatous cells. (a) EMSAs of nuclear extracts from lymphomatous cells of transgenic mice and a positive control, the Epstein-Barr virus–transformed lymphoid cell line, and normal mouse PBMCs with a radiolabed NF-κB binding oligonucleotide probe. Specific shifted bands of NF-κB binding proteins (arrow) were exclusively detected in nuclear extracts from lymphoblastoid cell line and transgenic mice with disease (Tg-L) in the presence of the competitor. (b) Supershift assay of nuclear extracts from Tg-L using antibodies against p50, p65, p52, and c-Rel. Normal IgG was used as control. Supershifted bands were detected in extracts with p50-specific and c-Rel–specific antibodies.

Flow cytometry. We performed flow cytometry with a FACSCalibur (BD Bioscience Clontech) using standard methods. Briefly, we prepared single-cell suspensions from spleen in PBS containing 2% FCS and 0.05% sodium azide. For detection of surface antigens, we washed cells and stained them with saturating amounts of antibodies conjugated with FITC, PE or APC in the presence of blocking antibody 2.4G2 (FcR-specific) monoclonal antibody for 20 min on ice. For analysis of live cells, we added propidium iodide at a final concentration of 5 μg/ml. For detection of intracellular CD3, we stained cells with ethidium monoazide bromide (5 μg/ml), fixed them with 4% formaldehyde in PBS and incubated them in permeabilization buffer containing 0.5% saponin. We incubated cells with FITC-conjugated CD3-specific antibody or control monoclonal antibody (rat IgG2b). We carried out analysis using the Cell Quest program and reanalyzed data using FlowJo software (Tree Star) by gating live cells. Specific monoclonal antibodies used are detailed in **Supplementary Methods** online.

Immunofluorescence studies of surface and cytoplasmic CD3 staining. We collected cells (10⁶) directly from spleen tissues from SCID mice, and washed and incubated them with CD3-specific antibody. Thereafter, we incubated samples with Alexa 488R–conjugated goat rabbit-specific IgG and then stained with propidium iodide (1 μg/ml). We permeabilized cells before incubation with primary antibody and detected immunofluorescent signals using a confocal microscope (IX70, Olympus).

epigenetic changes that restrict viral gene expression, but it is presently unclear whether such changes might at some point develop in this transgenic mouse model.

The models of ATLL developed in both transgenic and SCID mice will now allow detailed investigation of the role of Tax and the identification of specific molecular events associated with transformation. Moreover, the rapid development of fulminant disease in SCID mice will uniquely facilitate the evaluation of a range of therapeutic interventions that may ultimately lead to more effective treatments of human disease.

METHODS

Details are in **Supplementary Methods** online.

Mice. All mouse experimental protocols were approved by the Animal Care and Use Committee of the National Institute of Infectious Diseases, Tokyo, Japan, and by the Animal Research Ethics Committee of University College Dublin, Ireland. We purchased C57BL/6 mice from Charles River and the Oriental Yeast Company. We obtained SCID mice from Clea Japan.

Plasmid construction and generation of transgenic mice. We generated transgenic mice using inbred C57BL/6 mice and standard methods. We prepared the transgene construct (pLck-Tax) by subcloning the HTLV-I Tax coding sequence into the BamHI site of p1017 (provided by R.M. Perlmutter, University of Washington). We amplified Tax cDNA by PCR from DNA extracted from infected peripheral blood mononuclear cells (PBMCs). The pLck-Tax plasmid was linearized by digestion with NotI (Boerhinger Mannheim), resulting in a 6.3-kb fragment containing the transgene, and this was purified using a Qiaex gel extraction kit (Qiagen) before injection. All mice were housed under specific pathogen-free conditions. Mice were killed after anesthesia with chloroform by syringe cardiac exsanguination. For detection of the transgene, we performed Southern blotting on genomic DNA extracted from tail-tip biopsies.

Chromosomal mapping of the inserted transgene. We identified genomic sequences flanking the transgenes by genomic walking methods[28] using the Universal Genome Walker kit (BD Bioscience Clontech) according to the manufacturer's instructions. Briefly, we constructed adaptor-ligated genomic

EMSAs. We prepared nuclear extracts from 1–10 × 10⁶ of lymphomatous cells from spleens of transgenic mice, an Epstein-Barr virus–transformed lymphoblastoid cell line, and PBMCs from control mice as previously described[29]. We performed an EMSA with the Gel Shift Assay Systems kit (Promega) according to the manufacturer's protocol. We separated samples by electrophoresis on 4% polyacrylamide gels in 0.25% Tris–boric acid–EDTA, and dried and analyzed them using a BAS 2000 image analyzer (Fujifilm).

Real-time quantitative PCR. We used real-time PCR (RT-PCR) to quantify expression of Tax mRNA in transgenic and SCID mice. We harvested spleens at birth and at 8 weeks, 11 weeks, 5 months, 18 months in transgenic mice without disease, and at 18 months in mice with leukemia-lymphoma, from control littermates and from SCID mice after intraperitoneal transfer of lymphomatous cells. We measured levels of Tax mRNA by RT-PCR after reverse transcription using the ABI PRISM 7900 sequence detection system (Applied Biosystems) with a QuantiTect Probe PCR kit (Qiagen).

Transfer of leukemia and lymphoma to SCID mice. We harvested spleen cells from transgenic mice and directly suspended them in RPMI medium. We directly injected cells (10⁶) intraperitoneally or intradermally into SCID mice

TECHNICAL REPORTS

from three individual transgenic animals. At 28 d, when mice were clearly ill, we carried out pathological and immunological studies as above.

Electron microscopy. We collected cells from ascites of SCID mice and fixed them in 2.5% glutaraldehye and 2% paraformaldehyde, postfixed them in 1% osmium tetroxide, dehydrated them and embedded them in epoxy resin. We stained ultrathin, 80-nm sections with uranyl and lead acetate and examined them with a JEM-1220 electron microscope (Jeol Datum) at 80 kV.

URL. Ensembl, http://www.ensembl.org

Note: Supplementary information is available on the Nature Medicine website.

1. Matsuoka, M. Human T-cell leukemia virus type I and adult T-cell leukemia. *Oncogene* **22**, 5131–5140 (2003).
2. Takatsuki, K. *et al.* Clinical diversity in adult T-cell leukemia-lymphoma. *Cancer Res.* **45**, 4644s–4645s (1985).
3. Hattori, T. *et al.* Leukaemia of novel gastrointestinal T-lymphocyte population infected with HTLV-I. *Lancet* **337**, 76–77 (1991).
4. Suzushima, H. *et al.* Double-negative (CD4- CD8-) T cells from adult T-cell leukemia patients also have poor expression of the T-cell receptor alpha beta/CD3 complex. *Blood* **81**, 1032–1039 (1993).
5. Kamihira, S. *et al.* Unusual morphological features of adult T-cell leukemia cells with aberrant immunophenotype. *Leuk. Lymphoma* **12**, 123–130 (1993).
6. Suzushima, H., Asou, N., Hattori, T. & Takatsuki, K. Adult T-cell leukemia derived from S100 beta positive double-negative (CD4- CD8-) T cells. *Leuk. Lymphoma* **13**, 257–262 (1994).
7. Shimauchi, T., Hirokawa, Y. & Tokura, Y. Purpuric adult T-cell leukaemia/lymphoma: expansion of unusual CD4/CD8 double-negative malignant T cells expressing CCR4 but bearing the cytotoxic molecule granzyme B. *Br. J. Dermatol.* **152**, 350–352 (2005).
8. Yamada, Y. *et al.* Adult T-cell leukemia with atypical surface phenotypes: clinical correlation. *J. Clin. Oncol.* **3**, 782–788 (1985).
9. Ohata, J. *et al.* CD4/CD8 double-positive adult T-cell leukemia with preceding cytomegaloviral gastroenterocolitis. *Int. J. Hematol.* **69**, 92–95 (1999).
10. Ciminale, V. *et al.* Unusual CD4+CD8+ phenotype in a Greek patient diagnosed with adult T-cell leukemia positive for human T-cell leukemia virus type I (HTLV-I). *Leuk. Res.* **24**, 353–358 (2000).
11. Uchiyama, T., Yodoi, J., Sagawa, K., Takatsuki, K. & Uchino, H. Adult T-cell leukemia: clinical and hematologic features of 16 cases. *Blood* **50**, 481–492 (1977).
12. Yoshida, M. Multiple viral strategies of HTLV-1 for dysregulation of cell growth control. *Annu. Rev. Immunol.* **19**, 475–496 (2001).
13. Jeang, K.T., Giam, C.Z., Majone, F. & Aboud, M. Life, death, and tax: role of HTLV-I oncoprotein in genetic instability and cellular transformation. *J. Biol. Chem.* **279**, 31991–31994 (2004).
14. Sun, S.C. & Yamaoka, S. Activation of NF-kappaB by HTLV-I and implications for cell transformation. *Oncogene* **24**, 5952–5964 (2005).
15. Hall, W.W. & Fujisawa, M. Deregulation of cell-signalling pathways in HTLV-I infection. *Oncogene* **24**, 5965–5975 (2005).
16. Nerenberg, M., Hinrichs, S.H., Reynolds, R.K., Khoury, G. & Jay, G. The tat gene of human T-lymphotropic virus type 1 induces mesenchymal tumors in transgenic mice. *Science* **237**, 1324–1329 (1987).
17. Hinrichs, S.H., Nerenberg, M., Reynolds, R.K., Khoury, G. & Jay, G. A transgenic mouse model for human neurofibromatosis. *Science* **237**, 1340–1343 (1987).
18. Green, J.E., Hinrichs, S.H., Vogel, J. & Jay, G. Exocrinopathy resembling Sjogren's syndrome in HTLV-1 tax transgenic mice. *Nature* **341**, 72–74 (1989).
19. Iwakura, Y. *et al.* Induction of inflammatory arthropathy resembling rheumatoid arthritis in mice transgenic for HTLV-I. *Science* **253**, 1026–1028 (1991).
20. Green, J.E., Baird, A.M., Hinrichs, S.H., Klintworth, G.K. & Jay, G. Adrenal medullary tumors and iris proliferation in a transgenic mouse model of neurofibromatosis. *Am. J. Pathol.* **140**, 1401–1410 (1992).
21. Grossman, W.J. *et al.* Development of leukemia in mice transgenic for the tax gene of human T-cell leukemia virus type I. *Proc. Natl. Acad. Sci. USA* **92**, 1057–1061 (1995).
22. Chaffin, K.E. *et al.* Dissection of thymocyte signaling pathways by *in vivo* expression of pertussis toxin ADP-ribosyltransferase. *EMBO J.* **9**, 3821–3829 (1990).
23. Wildin, R.S. *et al.* Developmental regulation of lck gene expression in T lymphocytes. *J. Exp. Med.* **173**, 383–393 (1991).
24. Mori, N. *et al.* Constitutive activation of NF-kappaB in primary adult T-cell leukemia cells. *Blood* **93**, 2360–2368 (1999).
25. Staal, F.J., Weerkamp, F., Langerak, A.W., Hendriks, R.W. & Clevers, H.C. Transcriptional control of T lymphocyte differentiation. *Stem Cells* **19**, 165–179 (2001).
26. Rezuke, W.N., Abernathy, E.C. & Tsongalis, G.J. Molecular diagnosis of B- and T-cell lymphomas: fundamental principles and clinical applications. *Clin. Chem.* **43**, 1814–1823 (1997).
27. Kannagi, M., Ohashi, T., Harashima, N., Hanabuchi, S. & Hasegawa, A. Immunological risks of adult T-cell leukemia at primary HTLV-I infection. *Trends Microbiol.* **12**, 346–352 (2004).
28. Noguchi, A. *et al.* Chromosomal mapping and zygosity check of transgenes based on flanking genome sequences determined by genomic walking. *Exp. Anim.* **53**, 103–111 (2004).
29. Dignam, J.D., Martin, P.L., Shastry, B.S. & Roeder, R.G. Eukaryotic gene transcription with purified components. *Methods Enzymol.* **101**, 582–598 (1983).

ELSEVIER

Brief communication

The permeability to water and cryoprotectants of immature and mature oocytes in the zebrafish (*Danio rerio*) ☆

Shinsuke Seki, Toshimitsu Kouya, Delgado M. Valdez Jr. , Bo Jin, Takao Hara, Naoya Saida, Magosaburo Kasai, Keisuke Edashige *

Laboratory of Animal Science, College of Agriculture, Kochi University, Nankoku, Kochi 783-8502, Japan

Abstract

To identify a stage feasible for the cryopreservation of zebrafish oocytes, we investigated the permeability to water and cryoprotectants of immature (stage III) and mature (stage V) oocytes. The permeability to water (μm/min/atm) of immature oocytes at 25 °C (0.37) was significantly higher than that of mature oocytes (0.10). The permeability ($\times 10^{-3}$ cm/min) of immature oocytes to ethylene glycol, propylene glycol, and Me_2SO (1.49–3.03) at 25 °C was substantially higher than that of mature oocytes ~0. The permeability of immature oocytes to glycerol was also high (1.75), although the permeability could not be measured in mature oocytes. Immature oocytes would be more suitable than mature oocytes for conservation of the zebrafish.
© 2006 Elsevier Inc. All rights reserved.

Keywords: Zebrafish; Oocyte; Permeability; Water; Cryoprotectant

Among teleosts, the zebrafish (*Danio rerio*) is an important experimental animal in developmental biology, genetics, and physiology. However, it has been maintained by mating because its embryos are unable to be cryopreserved. Because fish embryos have a large size (resulting in a low surface area/volume ratio), a large amount of egg-yolk, and a thick chorion, and form a complex structure during development, it is difficult to cryopreserve them. However, zebrafish oocytes constitute a single compartment and do not have barriers to permeability like the multinucleated yolk syncytial layer found in zebrafish embryos [4]. These features would be advantageous for cryopreservation. Since zebrafish sperm can be cryopreserved easily [1], the long-term preservation of various stocks of zebrafish could be realized if their oocytes could be cryopreserved. To cryopreserve zebrafish oocytes successfully, it is important to

know the stage of maturation most feasible for cryopreservation. In the medaka, another small freshwater fish, we have found that the permeability of immature oocytes to water and cryoprotectants is remarkably higher than that of mature oocytes [8]. Considering their huge embryos/oocytes, rapid permeation of cryoprotectants is favored for successful cryopreservation. Very recently, Zhang et al. reported that the permeability of immature zebrafish oocytes to propylene glycol and Me_2SO was high [11]. A similar change might be observed in zebrafish oocytes.

In this study, we tried to determine the permeability to water and four major cryoprotectants (ethylene glycol, glycerol, propylene glycol, and Me_2SO) of immature and mature zebrafish oocytes to find the most feasible stage of maturation and suitable cryoprotectants for cryopreservation.

About 20–40 mature female zebrafish, purchased from a local fish dealer, were maintained in 60-l aquaria under 14-h light and 10-h dark periods at 28 °C. To obtain immature oocytes at the stage III of maturation, mature female zebrafish were killed by decapitation under anesthesia with 0.2 mg/ml of tricaine in distilled water (tricaine solution).

 * Corresponding author. Fax: +81 88 864 5200.
   E-mail address: keisuke@cc.kochi-u.ac.jp (K. Edashige).

The ovaries were recovered and placed in a 75% Leibovitz L-15 medium (pH 7.5) containing 100 μg/ml of gentamycin sulfate at 25 °C, and follicles were separated manually with forceps and scissors. The size of the follicles was measured under a microscope and follicles 0.60–0.69 mm in diameter were collected and used as immature oocytes. Mature oocytes at the stage V were obtained by squeezing the belly of mature females under anesthesia with the tricaine solution at about 30 min before the end of the dark period. The mature oocytes were placed in 4 ml of the 75% Leibovitz L-15 medium at 25 °C until used for experiments.

In this study, we assumed that the osmolality of the oocyte cytoplasm was equilibrated with the 75% Leibovitz L-15 medium (0.24 Osm/kg), because, until used for experiments, immature and mature oocytes were incubated in this medium for at least 60 min; it is sufficient for the oocytes to be equilibrated with the 75% Leibovitz L-15 medium. In fact, there is no volume change in immature and mature oocytes after equilibration for 60 min (data not shown). Then, the oocytes were transferred to the same medium containing 0.15, 0.48, or 0.74 M sucrose (total osmolality being 0.40, 0.80, and 1.20 Osm/kg, respectively), or in a 50% or 60% Leibovitz L-15 medium (0.16 and 0.19 Osm/kg, respectively) diluted with distilled water, with a minimal amount of the 75% Leibovitz L-15 medium using a pipette, and kept at 25 ± 0.5 °C for 60 min. The osmolality contributed by sucrose was calculated from published data on the colligative properties of sucrose in aqueous solutions [9]. The osmolality of the 50, 60, and 75% Leibovitz L-15 media was measured with a freezing point depression osmometer (OM801; Vogel, Giessen, Germany). Microscopic images of the oocytes were recorded using a time-lapse video recorder (ETV-820, Sony, Tokyo, Japan) for 60 min during exposure. The cross-sectional area of the oocytes was measured using an image analyzer (VM-50, Olympus, Tokyo, Japan). Relative cross-sectional area, S, was expressed by dividing the cross-sectional area by the initial area of the same oocyte. The relative volume (V) was obtained from $V = S^{3/2}$. Osmotically inactive fractions (V_b) were obtained from Boyle–van't Hoff plots of the relative volumes of oocytes after exposure to solutions with various osmolalities for 60 min.

To determine the permeability to water and cryoprotectants from the volume changes, an oocyte equilibrated with the 75% Leibovitz L-15 medium at 25 °C for at least 60 min was introduced into the same medium containing sucrose or one of the cryoprotectants (200 μl) covered with paraffin oil in a Petri dish (35 × 10 mm), and kept at 25 ± 0.5 °C for 60 min. Microscopic images of the oocyte were recorded using the time-lapse video recorder for 60 min. The cross-sectional area of the oocyte was measured and the relative volume at various time points of exposure was calculated as described above. Water-permeability (Lp) and cryoprotectant-permeability (Ps) were determined by fitting water and solute movements using a two-parameter formalism [7,2,8]. The Lp of immature and mature oocytes was determined from volume changes in the 75% Leibovitz L-15 medium

containing 0.15 M sucrose (total osmolality being 0.40 Osm/kg). The Ps of oocytes for each cryoprotectant was calculated from their volume changes in a 75% Leibovitz L-15 media containing 8% (v/v) ethylene glycol, 10% (v/v) glycerol, 10% (v/v) propylene glycol, or 9.5% (v/v) Me$_2$SO at 25 ± 0.5 °C for 60 min. The total osmolality of the 75% Leibovitz L-15 medium containing 8% ethylene glycol, 10% glycerol, 10% propylene glycol, and 9.5% Me$_2$SO was 1.85, 1.83, 1.80, and 1.79 Osm/kg, respectively. The osmolality of the 75% Leibovitz L-15 medium was 0.24 Osm/kg. Different concentrations of cryoprotectants were used to give cryoprotectant solutions a similar osmolality (about 1.8 Osm/kg). The osmolality of ethylene glycol, glycerol, and propylene glycol was calculated from published data on the colligative properties of each cryoprotectant in aqueous solutions [9]. The osmolality of 9.5% Me$_2$SO in an aqueous solution was measured with a vapor pressure osmometer (Vapro 5520, Wescor, Logan, UT, USA). Other constants were as follows; gas constant (R), 8.206 10^{-2} liter atm/K/mol; absolute temperature (T), 298 K; partial molar volume of water (V_W), ethylene glycol (V_{EG}), glycerol (V_{GLY}), propylene glycol (V_{PG}), and Me$_2$SO (V_{Me2SO}), 0.018, 0.054, 0.071, 0.070, and 0.069 L/mol, respectively [9,6].

To determine the permeability to water and cryoprotectants, the V_b values of immature oocytes and mature oocytes were calculated. Fig. 1 shows the Boyle–van't Hoff plots of immature and mature oocytes. Immature oocytes shrunk or swelled according to the osmolality of solutions (0.16 to 0.40 Osm/kg), but the plasma membrane of immature oocytes was ruptured during the exposure in solutions with an osmolality of 0.80 Osm/kg or more. A linear Boyle–van't Hoff relationship was observed in immature oocytes ($r^2 = 0.99$). Mature oocytes also shrunk in hypertonic
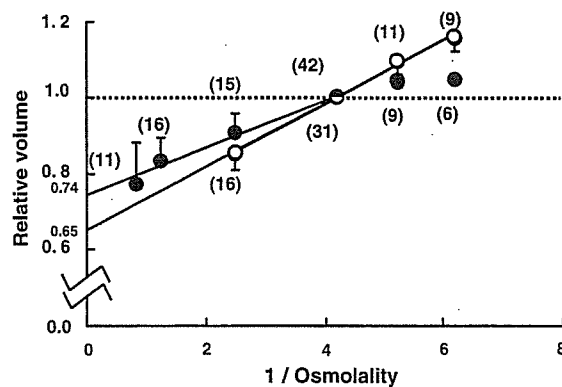
Fig. 1. Boyle–van't Hoff plots of relative volumes of immature (open) and mature (closed) zebrafish oocytes. Both immature and mature oocytes were equilibrated with a 75% Leibovitz L-15 medium. Then, immature oocytes were equilibrated with a 75% Leibovitz L-15 medium containing 0.15 M sucrose (0.40 Osm/kg) or with a 50% or 60% Leibovitz L-15 medium (0.16 and 0.19 Osm/kg, respectively) diluted with distilled water at 25 °C for 60 min. Mature oocytes were equilibrated with a 75% Leibovitz L-15 medium containing 0.48 M or 0.74 M sucrose (0.80 and 1.20 Osm/kg, respectively) or with a 50% or 60% Leibovitz L-15 medium diluted with distilled water at 25 °C for 60 min. Data are indicated as means of relative volumes ± SD. Numbers in parentheses indicate the number of oocytes used.

sucrose solutions in response to the osmolality of the solutions, but mature oocytes did not swell in hypotonic solutions. Similar phenomenon in hypotonic solutions have been reported in zebrafish embryos [5]. Since freshwater fish spawn in freshwater where the oocytes are then fertilized and develop, mature oocytes and embryos must acquire the resistance to hypotonic conditions [8]. Fortunately, mature oocytes shrunk in hypertonic solutions in response to the osmolality of solutions. Moreover, the membrane-permeability in hypertonic solutions is important, because for cryopreservation, the cells are exposed to a cryoprotectant solution having very high osmolality. Thus, we determined the V_b of mature oocytes from relative volume in hypertonic solutions (0.24 to 1.20 Osm/kg, $r^2 = 0.97$). The V_b value was 0.65 for immature oocytes and 0.74 for mature oocytes. Zhang and colleagues estimated the V_b of immature and mature oocytes to be 0.70 and 0.64, respectively, from their relative volumes in 'hypertonic conditions' [10,11]. These values are similar to the ones obtained in the present study. We used our values to determine the permeability to water and cryoprotectants of oocytes.

Immature oocytes shrunk rapidly in the 0.15 M sucrose solution (0.40 Osm/kg), but mature oocytes shrunk slowly (Fig. 2A). The Lp (µm/min/atm) value of immature oocytes (0.37) calculated from the data was markedly higher than that of mature oocytes (0.10) (Table 1). This shows that water permeates immature oocytes much faster than mature oocytes. It has been shown in zebrafish embryos that the Lp is low; 0.02–0.05 µm/min/atm, assuming that the initial internal osmolality is 0.04 Osm/kg, and 0.04–0.10 µm/min/atm, assuming that the initial internal osmolality is 0.30 Osm/kg at the six-somite stage [3]. Therefore, their higher permeability to water makes immature oocytes more attractive than mature oocytes and embryos for cryopreservation.

Figs. 2B–E shows the changes in volume of immature oocytes and mature oocytes at 25 °C in the 75% Leibovitz L-15 medium containing ethylene glycol, glycerol, propylene glycol, or Me₂SO. In all of these solutions, immature oocytes shrunk and regained their volume within 60 min, suggesting that the cryoprotectants permeated immature oocytes efficiently. On the other hand, mature oocytes shrunk very slowly and did not regain their volume during 60 min of exposure in the solution with ethylene glycol, propylene glycol, or Me₂SO, suggesting that these cryoprotectants permeate mature oocytes quite slowly. In the glycerol solution (Fig. 2C), mature oocytes shrunk and ruptured within 15 min of exposure.

The L_p (µm/min/atm) of immature oocytes in various cryoprotectants (0.17–0.28) was markedly higher than that of mature oocytes (0.03–0.05), and no marked difference in the Lp values of immature oocytes was observed among cryoprotectant solutions (Table 1). The values were slightly lower than the value in hypertonic sucrose solutions (0.37). Ps values ($\times 10^{-3}$ cm/min) of immature oocytes for ethylene glycol, glycerol, propylene glycol, and Me₂SO were 2.80, 1.75, 1.49, and 3.03, respectively (Table 1). As far as we
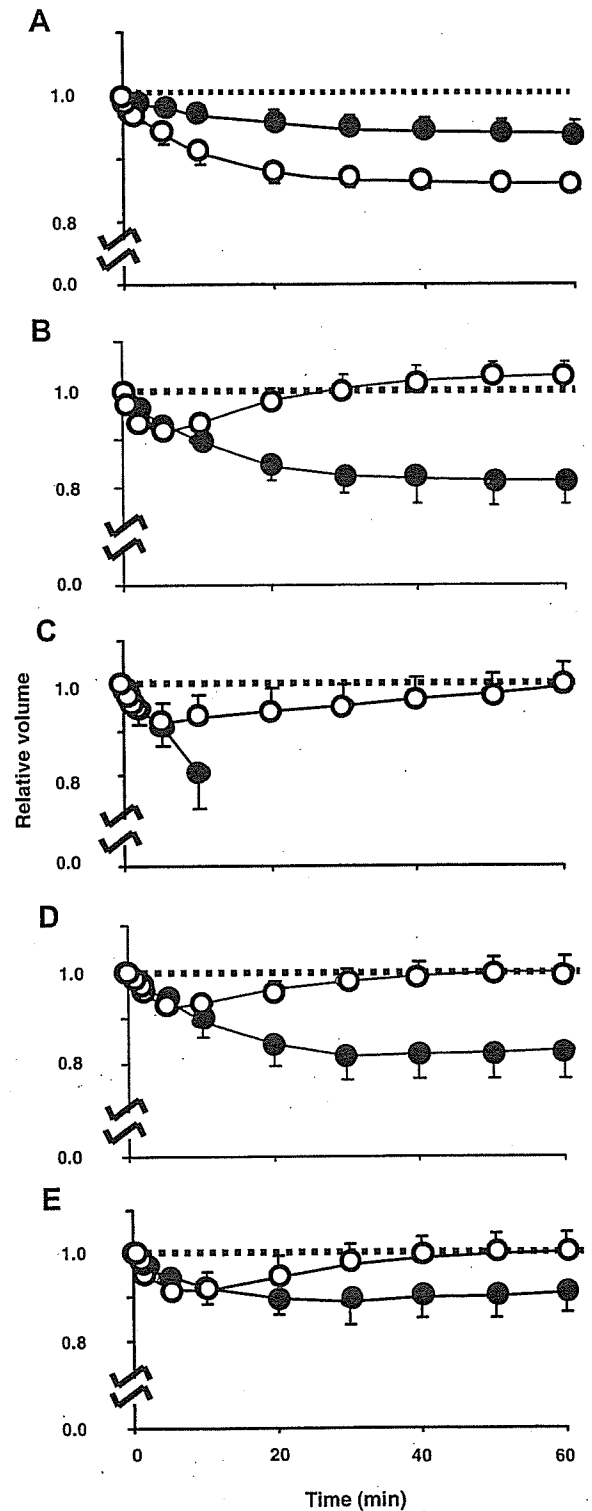
Fig. 2. Changes in cell volume of immature (open) and mature (closed) zebrafish oocytes in a 75% Leibovitz L-15 medium containing 0.15 M sucrose (A), 8% (v/v) ethylene glycol (B), 10% (v/v) glycerol (C), 10% (v/v) propylene glycol (D), or 9.5% (v/v) Me₂SO (E) at 25 °C for 60 min. Data are indicated as means of relative volumes ± SD. Data for immature oocytes were from 8 to 10 oocytes, and those for mature oocytes were from 4 to 12 oocytes.

Table 1
The permeability of zebrafish oocytes to water (Lp, μm/min/atm) and cryoprotectants (Ps, $\times 10^{-3}$ cm/min)

Oocytes	Permeability	Permeabilities of oocytes in solutions with				
		0.15 M Suc[a]	8%EG[b]	10%Gly[c]	10%PG[d]	9.5%Me$_2$SO
Immature (stage III)	Lp	0.37 ± 0.08	0.27 ± 0.10	0.17 ± 0.07	0.17 ± 0.06	0.28 ± 0.08
	Ps	—	2.80 ± 1.38	1.75 ± 1.67	1.49 ± 0.67	3.03 ± 1.92
Mature (stage V)	Lp	0.10 ± 0.09	0.03 ± 0.01^e	nd[f]	0.03 ± 0.01^e	0.05 ± 0.01^e
	Ps	—	~0	nd[f]	~0	~0

[a] Sucrose.
[b] Ethylene glycol.
[c] Glycerol.
[d] Propylene glycol.
[e] Lp values were estimated, assuming that Ps values were 0.
[f] Not determined.

know, this is the first report to determine the permeability of zebrafish oocytes to ethylene glycol and glycerol. On the other hand, Ps values of mature oocytes were too low to be determined from the volume changes (Fig. 2, Table 1). Similar changes in permeability to cryoprotectants were observed in medaka oocytes [8]. Therefore, during maturation, oocytes of freshwater fish must become less permeable to water and to small neutral solutes, probably by acquiring resistance to hypotonic conditions before being spawned in freshwater. Hagedorn et al. reported that the permeability of zebrafish embryos to propylene glycol and to Me$_2$SO was quite low [4]. Thus, not only mature oocytes but also embryos are less permeable to cryoprotectants than immature oocytes. The higher cryoprotectant-permeability of immature oocytes would also be an advantage over mature oocytes and embryos.

In this study, we showed that ethylene glycol and Me$_2$SO permeate immature oocytes more efficiently than other cryoprotectants. Therefore, in terms of permeability, ethylene glycol and Me$_2$SO would be more suitable for cryopreservation than glycerol and propylene glycol. Very recently, Zhang et al. reported the permeability of immature zebrafish oocytes to water (μm/min/atm) and to cryoprotectants ($\times 10^{-3}$ cm/min) in solutions with propylene glycol (Lp, 0.20; P_{PG}, 0.93) and Me$_2$SO (Lp, 0.17; P_{Me2SO}, 0.95) at 22 °C [11]. The Lp values in the propylene glycol solution and Me$_2$SO solution in the present study are similar to those in their report, but their values were lower (P_{PG}, 1.49; P_{Me2SO}, 3.03) (Table 1). This might be caused by the difference in temperature; Ps was measured at 25 °C in the present study but versus 22 °C in Zhang et al.'s study.

In this study, we determined the permeability of mature oocytes, although Zhang et al. reported that they could not determine the permeability, because the change in volume was only slight and untheoretical in solutions with 2 M propylene glycol or 2 M Me$_2$SO [11]. When we examined the volume changes of mature oocytes under the same conditions as in their study (not described), we often observed a similar phenomenon, but this phenomenon occurred only in about 10–20% of mature oocytes both in the additional study and in the present study. Most mature oocytes usually shrunk and swelled in cryoprotectant solutions, and the

volume changes fitted well with the simulated curves for the oocytes. The difference in the strain of zebrafish might be involved in this discrepancy.

In conclusion, as observed in medaka oocytes, immature oocytes would be more suitable for cryopreservation than mature oocytes and embryos in the zebrafish. In addition, ethylene glycol and Me$_2$SO would be suitable cryoprotectants for cryopreservation, from the viewpoint of permeability.

References

[1] M. Brand, M. Granato, C. Nusslein-Volhard, Keeping and raising zebrafish, in: C. Nusslein-Volhard, R. Dahm (Eds.), Zebrafish, Oxford University Press, New York, 2002, pp. 30–34.
[2] K. Edashige, Y. Yamaji, F.W. Kleinhans, M. Kasai, Artificial expression of aquaporin-3 improves the survival of mouse oocytes after cryopreservation, Biol. Reprod. 68 (2003) 87–94.
[3] M. Hagedorn, E. Hsu, F.W. Kleinhans, D.E. Wildt, New approaches for studying the permeability of fish embryos: toward successful cryopreservation, Cryobiology 34 (1997) 335–347.
[4] M. Hagedorn, F.W. Kleinhans, D. Artemov, U. Pilatus, Characterization of a major permeability barrier in the zebrafish embryo, Biol. Reprod. 59 (1998) 1240–1250.
[5] M. Hagedorn, S.L. Lance, D.M. Fonseca, F.W. Kleinhans, D. Artimov, R. Fleischer, A.T.M.S. Hoque, M.B. Hamilton, B.S. Pukazhenthi, Altering fish embryos with aquaporin-3: an essential step toward successful cryopreservation, Biol. Reprod. 67 (2002) 961–966.
[6] O. Kiyohara, G. Perron, J.E. Desnoyers, Volumes and heat capacities of dimethylsulfoxide, acetone, and acetamide in water and of some electrolytes in these mixed aqueous solvents, Can. J. Chem. 53 (1975) 3263–3268.
[7] F.W. Kleinhans, Membrane permeability modeling: Kedem–Katchalsky vs a two-parameter formalism, Cryobiology 37 (1998) 271–289.
[8] D.M. Valdez, A. Miyamoto, T. Hara, S. Seki, M. Kasai, K. Edashige, Water- and cryoprotectant-permeability of mature and immature oocytes in the medaka (Oryzias latipes), Cryobiology 50 (2005) 93–102.
[9] A.V. Wolf, M.G. Brown, P.G. Prentiss, Concentration properties of aqueous solutions: conversion tables, in: R.C. Weast (Ed.), Handbook of Chemistry and Physics, fifty first ed., Chemical Rubber Co., Cleveland, 1970, pp. D181–D226.
[10] T. Zhang, D.M. Rawson, Permeability of dechorionated one-cell and six-somite stage zebrafish (Brachydanio rerio) embryos to water and methanol, Cryobiology 37 (1998) 13–21.
[11] T. Zhang, A. Isayeva, S.L. Adams, D.M. Rawson, Studies on membrane permeability of zebrafish (Danio rerio) oocytes in the presence of different cryoprotectants, Cryobiology 50 (2005) 285–293.

Channel-Dependent Permeation of Water and Glycerol in Mouse Morulae[1]

Keisuke Edashige,[2,3] Mitsunobu Tanaka,[3] Natsuko Ichimaru,[3] Satoshi Ota,[3] Ken-ichi Yazawa,[3]
Yuki Higashino,[3] Megumi Sakamoto,[3] Yohei Yamaji,[3] Tatsunaga Kuwano,[3] Delgado M. Valdez Jr.,[3]
F.W. Kleinhans,[4] and Magosaburo Kasai[3]

Laboratory of Animal Science,[3] College of Agriculture, Kochi University, Nankoku, Kochi 783-8502, Japan
Department of Physics,[4] Indiana University and Purdue University Indianapolis, Indianapolis, Indiana 46202

ABSTRACT

The cryosensitivity of mammalian embryos depends on the stage of development. Because permeability to water and cryoprotectants plays an important role in cryopreservation, it is plausible that the permeability is involved in the difference in the tolerance to cryopreservation among embryos at different developmental stages. In this study, we examined the permeability to water and glycerol of mouse oocytes and embryos, and tried to deduce the pathway for the movement of water and glycerol. The water permeability (L_p, μm min^{-1} atm^{-1}) of oocytes and four-cell embryos at 25°C was low (0.63–0.70) and its Arrhenius activation energy (E_a, kcal/mol) was high (11.6–12.3), which implies that the water permeates through the plasma membrane by simple diffusion. On the other hand, the L_p of morulae and blastocysts was quite high (3.6–4.5) and its E_a was quite low (5.1–6.3), which implies that the water moves through water channels. Aquaporin inhibitors, phloretin and p-(chloromercuri) benzene-sulfonate, reduced the L_p of morulae significantly but not that of oocytes. By immunocytochemical analysis, aquaporin 3, which transports not only water but also glycerol, was detected in the morulae but not in the oocytes. Accordingly, the glycerol permeability (P_{GLY}, $\times 10^{-3}$ cm/min) of oocytes was also low (0.01) and its E_a was remarkably high (41.6), whereas P_{GLY} of morulae was quite high (4.63) and its E_a was low (10.0). Aquaporin inhibitors reduced the P_{GLY} of morulae significantly. In conclusion, water and glycerol appear to move across the plasma membrane mainly by simple diffusion in oocytes but by facilitated diffusion through water channel(s) including aquaporin 3 in morulae.

embryo, developmental biology, ovum

INTRODUCTION

Since the first successful cryopreservation of mouse embryos in 1972 [1], various protocols have been developed to cryopreserve oocytes and embryos of many mammalian species. However, it is difficult to obtain high survival rates of embryos at different stages with a single cryopreservation protocol. For example, mouse morulae can be cryopreserved without appreciable loss of viability by a simple one-step vitrification method using an ethylene glycol-based solution [2], but pretreatment with a lower concentration of cryopro-

tectant is needed to vitrify mouse embryos at early stages [3]. This indicates that cryobiological properties differ among embryos at different developmental stages.

There are many factors that affect the survival of cells after cryopreservation [4]. Plasma membrane permeability is one factor determining the tolerance of cells to cryopreservation because the permeability modulates several major forms of cell injury caused by cryopreservation, i.e., injuries by intracellular ice formation, cryoprotectant toxicity, and osmotic swelling. Thus, it is likely that the plasma membrane permeability markedly differs among embryos at different developmental stages and with different cryosensitivities.

Water was long believed to move across the plasma membrane only by simple diffusion. In the 1990s, however, small intrinsic membrane proteins that act as water channels, called aquaporins (AQPs), were discovered and characterized [5]. We have already demonstrated that mRNAs of *Aqp3* and *Aqp7* are present in mouse oocytes at the metaphase II stage and embryos at the four-cell, morula, and blastocyst stages, and that mRNAs of *Aqp8* and *Aqp9* are expressed in embryos at the blastocyst stage [6]. Other researchers have also detected mRNAs of *Aqps* [7, 8] and AQP proteins [9] in mouse embryos. Thus, it is plausible that these AQPs play a role in the water permeability of mouse oocytes and embryos. However, it has not been shown whether such a channel pathway is a significant one in mouse oocytes and embryos.

The involvement of water channels in water movement across the plasma membrane can be deduced from the membrane's properties. In general, an osmotic water permeability higher than 4.5 μm min^{-1} atm^{-1} (or $P_f \geq 0.01$ cm/sec) and an Arrhenius activation energy (E_a) lower than 6 kcal/mol are suggestive of water movement principally through water channels, whereas an E_a higher than 10 kcal/mol is suggestive of movement principally via channel-independent diffusion [10]. Thus, it would be possible to deduce the pathway of movement from the water permeability and its E_a value.

If this criterion is applied to mature mouse oocytes, water channels may not be the major pathway for water movement across the plasma membrane because many studies have already shown that mouse oocytes have low water permeability (0.41–0.61 μm min^{-1} atm^{-1}) [11–16] and high E_a values (9.84–13.3 kcal/mol) [11–13, 17], although mouse oocytes have mRNAs of *Aqp3* and *Aqp7* [6]. They could be maternal stores of mRNA to be expressed later. Thus, most water molecules are assumed to move across the plasma membrane of oocytes by simple diffusion. In mouse embryos after cleavage, on the other hand, only a small number of studies have been available about the permeability of the plasma membrane. Pfaff et al. [16] estimated the water permeability of oocytes and embryos from the one-cell to eight-cell stage and demonstrated that eight-cell embryos are slightly more permeable to water than oocytes and one- to four-cell embryos, suggesting that water channels do not play a major role in

water movement in embryos until the eight-cell stage. However, the water permeability of embryos at later stages has not been studied.

In this study, we first examined the water permeability of mouse oocytes and embryos and temperature dependence to deduce the involvement of water channels in water movement. Because the results of this experiment suggested the involvement of a water channel that can transport not only water but also glycerol in embryos at later developmental stages, we also examined the glycerol permeability of oocytes and morulae and temperature dependence to deduce the involvement of channels in glycerol movement.

MATERIALS AND METHODS

Collection of Oocytes and Embryos

Female ICR mice (CLEA Japan, Inc., Tokyo, Japan) were induced to superovulate with intraperitoneal injections of 5 IU of eCG and 5 IU of hCG given 48 h apart, and were mated with male ICR mice. Ovulated unfertilized oocytes were collected from the ampullar portion of the oviducts at 13 h after hCG injection without mating and were freed from cumulus cells by suspending them in modified phosphate-buffered saline (PB1) containing 145 U/ml hyaluronidase followed by washing with fresh PB1 medium. Four-cell embryos were flushed from the oviducts of mated animals with PB1 medium 55 h after hCG injection. Morulae were collected from the uteri by flushing them with PB1 medium 76 h after hCG injection, and only compacted morulae were used. To obtain early blastocysts, morulae collected 76 h after hCG injection were cultured in modified M16 medium supplemented with 10 μM EDTA, 1 mM glutamine, and 10 μM β-mercaptoethanol (modified M16 medium) [18], covered with paraffin oil for 6–8 h in a humidified CO_2 incubator equilibrated with 5% CO_2 in air at 37°C. Only early blastocysts, with a blastocoele larger than the inner cell mass and an unexpanded zona pellucida, were collected. To measure total cell volume of blastocysts, the blastocysts were pipetted repeatedly with a narrow-bore pipette to shrink their blastocoele. After being pipetted, early blastocysts with a shrunken blastocoele were incubated in modified M16 medium in a CO_2 incubator for 4–5 min and those without a re-expanded blastocoele were used for experiments. All experiments were approved by the Animal Ethics Committee of Kochi University.

Measurement of Water Permeability and Glycerol Permeability of Mouse Oocytes and Embryos

Water permeability was measured as described previously [19, 20]. Each oocyte or embryo was placed in a 100-μl drop of PB1 medium covered with paraffin oil in a Petri dish (90 × 10 mm) at 25°C and was held by a holding pipette (outer diameter being 80–120 μm) connected to a micromanipulator on an inverted microscope. The inner diameter of the holding pipette was small enough not to distort the oocyte or embryo. The temperature of the paraffin oil covering the various solutions was considered as the temperature of the solutions and was kept at 25 ± 1°C by controlling the temperature of the room. An oocyte or embryo held by a holding pipette was then covered with a covering pipette with a larger inner diameter (~200 μm) connected to another micromanipulator. Then, by sliding the dish, the oocyte or embryo was introduced into a drop of hypertonic PB1 medium containing sucrose (100 μl) at 25°C. By removing the covering pipette, the oocyte or embryo was abruptly exposed to the solution. The microscopic image of the oocytes and embryos during exposure to the solution was recorded with a time-lapse video tape recorder (ETV-820; Sony, Tokyo, Japan) every 0.5 sec. The cross-sectional area of oocytes and embryos was measured using an image analyzer (VM-50; Olympus, Tokyo, Japan). In the case of four-cell embryos, the cross-sectional area of only one blastomere in each embryo was measured. The cross-sectional area was expressed as a relative cross-sectional area, S, by dividing it by the area of the same oocyte and embryo in isotonic PB1 medium. The relative volume was obtained from $V = S^{3/2}$.

The osmotically inactive portion (V_b) of oocytes and embryos is required for the permeability analysis. To determine V_b, they were exposed to PB1 medium (0.295 Osm/kg) containing 0.110, 0.310, or 0.505 Osm/kg sucrose at 25°C for 60 min; the total osmolalities of the solutions were 0.405, 0.605, and 0.800 Osm/kg, respectively. Values for V_b were obtained from Boyle-van't Hoff plots.

The water permeability of oocytes and embryos was determined by measuring the shrinkage of oocytes and embryos after their transfer from isotonic PB1 medium to PB1 medium containing 0.505 Osm/kg sucrose (total

osmolality, 0.800 Osm/kg) (sucrose/PB1) for 5 min at 25°C. In this study, we expressed water permeability as hydraulic conductivity (L_p). L_p values of the oocytes and embryos were determined by fitting water movement using a two-parameter formalism as described previously [19, 21]. The related constants and parameters used are listed in Table 1.

The L_p of oocytes and embryos was also measured at 15°C for 5 min, and the Arrhenius activation energy, E_a, or temperature dependence of L_p at each stage was obtained from Arrhenius plots.

In one experiment, oocytes and morulae were treated with phloretin or p-(chloromercuri) benzene-sulfonate (p-CMBS), which are AQP inhibitors, before water permeability was measured to study whether channels sensitive to these inhibitors were involved in water movement in oocytes and morulae. For this experiment, the water permeability of untreated oocytes and morulae was first measured at 25°C as described above, then the oocytes and morulae were transferred to PB1 medium and equilibrated for 10 min at 25°C. Next, they were treated with a water-channel inhibitor, 0.7 mM phloretin in PB1 medium for 2.5 min or 0.5 mM p-CMBS in PB1 medium for 30 min at 25°C. Finally, they were washed with PB1 medium, and water permeability was remeasured for 5 min at 25°C as described above.

The glycerol-permeability (P_{GLY}) of oocytes and embryos was determined by measuring the shrinkage and swelling of oocytes and embryos after transfer from isotonic PB1 medium to PB1 medium containing 10% (vol/vol) glycerol (1.565 Osm/kg) (total osmolality, 1.860 Osm/kg) (glycerol/PB1) for 20 min at 25°C. Values for S and V were obtained, and the P_{GLY} of the oocytes and embryos was determined by fitting water and solute movement using a two-parameter formalism as described above.

The P_{GLY} of oocytes and morulae was also measured at 15 and 25°C for 180 min and 5 min, respectively, and the Arrhenius activation energy of the P_{GLY} for oocytes and morulae was obtained, as for the water permeability.

For the study of effects of AQP inhibitors on the glycerol permeability of morulae, the glycerol permeability of untreated morulae was first measured in glycerol/PB1 for 5 min at 25°C as described above, then the morulae were diluted with PB1 medium containing 0.5 M sucrose for 20 min at 25°C, and equilibrated with fresh PB1 medium for 10 min at 25°C. Next, they were treated with a water-channel inhibitor in PB1 medium using the same conditions as for water permeability, washed with PB1 medium, and the permeability remeasured in glycerol/PB1 for 5 min at 25°C.

The osmolality of sucrose and glycerol (the osmolality of extracellular permeating solute) was calculated from published data about colligative properties of sucrose and glycerol in aqueous solutions [22]. The osmolality of PB1 medium (isotonic buffer) was measured with an osmometer (OM801; Vogel, Giessen, Germany).

In this report, we limited data collection to cells in the following volume ranges (before treatment): oocytes, 1.9–2.7 × 10E5 μm³ (95% of all oocytes used); blastomeres of four-cell embryos, 0.5–0.7 × 10E5 μm³ (92% of all four-cell embryos used); and morulae, 1.7–2.5 × 10E5 μm³ (82% of all morulae used) because the equilibrated relative volume of extraordinarily larger or smaller oocytes and embryos in hypertonic sucrose solutions had smaller or larger V_b values than that of those with an ordinary size, suggesting that such extraordinarily large or small oocytes and embryos have different V_b values from ordinary ones (data not shown). For early blastocysts, however, we used all of the data because the size of blastocysts with a shrunken blastocoele varied greatly, probably due to the variable size of the blastocoele.

Expression of AQP3 and AQP7 in Oocytes and Morulae

For detection of AQP3, we used commercially available anti-human AQP3 goat antibody (Santa Cruz Biotechnology, Inc., Santa Cruz, CA), which cross-reacted with mouse AQP3. For AQP7, rabbit anti-mouse AQP7 serum was raised against a synthetic peptide (Asahi Techno Glass; Chiba, Japan) corresponding to the 15 C-terminal amino acids of mouse AQP7 (KNAASA-NISGSVPLE) (GenBank accession number AB010100). Using an ECL

TABLE 1. Constant and parameters used for fitting permeability parameters.

Symbol	Meaning	Values
R	Gas constant	8.206×10^{-2} L atm $K^{-1}mol^{-1}$
T	Absolute temperatures	288 K and 298 K
$\overline{V_w}$	Partial molar volume of water	0.018 L/mol
$\overline{V_s}$	Partial molar volume of glycerol	0.071 L/mol[a]
V_b	Osmotically inactive fraction	—

[a] Value from Wolf et al. [22].

Western Blotting Kit (Amersham Biosciences Corp., Piscataway, NJ), we confirmed that the antiserum detected a 21-kDa protein in the membrane fraction of mouse kidney, which was consistent with the molecular weight of mouse AQP7, on a polyvinylidene fluoride membrane after electric transfer from an SDS-PAGE gel.

The zona pellucida of oocytes and morulae was removed by brief exposure to an acidic Tyrode solution (pH 2.5) [23]. The zona-free oocytes and morulae were fixed with a 2% paraformaldehyde solution containing 0.01 M sodium metaperiodate, 0.075 M lysine, and 0.075 M phosphate buffer (pH 7.4) at 4°C for 60 min. After being washed with PBS containing 5 mg/ml bovine serum albumin, they were permeabilized with PBS containing 0.25% Triton X-100. Then they were incubated with blocking solution; PBS containing 10% nonimmune donkey serum (Santa Cruz Biotechnology, Inc.) and 5 mg/ml bovine serum albumin (for AQP3) or 10% nonimmune goat serum (Santa Cruz Biotechnology, Inc.) and 5 mg/ml bovine serum albumin (for AQP7) at 25°C for 60 min. After being rinsed, they were incubated with diluted anti-human AQP3 goat antibody (1/400) or anti-mouse AQP7 rabbit antiserum with blocking solution at 25°C for 60 min. As a control, instead of the primary antibodies, anti-human AQP3 goat antibody or anti-mouse AQP7 rabbit antiserum preincubated with a blocking peptide, which was the same peptide used for an antigen, at room temperature for 1 h, was used for the experiments. After being rinsed, the oocytes and embryos were incubated with diluted fluorescein isothiocyanate (FITC)-conjugated anti-goat IgG donkey antibody (1/1600) (Santa Cruz Biotechnology, Inc.) (for AQP3) or diluted FITC-conjugated anti-rabbit IgG goat antibody (Chemicon International, Temecula, CA) (for AQP7) with blocking solution at 25°C for 30 min. They were observed under a fluorescence microscope. No staining was observed when primary antibodies preincubated with blocking peptides were used (data not shown). When cross sections of mouse kidney and testis that were fixed with paraformaldehyde, dehydrated with ethanol, embedded in paraffin, and cut at a thickness of 7 μm were stained with the same antibodies at the same dilution, the collecting duct or seminiferous epithelium was stained with anti-AQP3 antibody or anti-AQP7 antibody, respectively, where the presence of AQP3 and AQP7 has been elucidated (data not shown) [24, 25].

RESULTS

Fraction of Osmotically Inactive Cell Content of Oocytes and Embryos

Figure 1 shows Boyle-van't Hoff plots of the relative volume of oocytes and embryos at various stages. The intercept of the regression line indicates osmotically inactive volumes for oocytes, four-cell embryos, morulae, and early blastocysts to be 15%, 16%, 15%, and 14%, respectively. We used these values to estimate the L_p and P_{GLY} of oocytes and embryos.

Water Permeability and Arrhenius Activation Energy of Oocytes and Embryos

In sucrose/PB1, oocytes and four-cell embryos shrank relatively slowly at 25°C, and shrank more slowly at 15°C than at 25°C (Fig. 2). On the other hand, morulae and early blastocysts shrank very rapidly at 15 and 25°C, the difference of the volume changes between the two temperatures being small (Fig. 2).

In oocytes and four-cell embryos, the value for L_p at 25°C was low (0.70 ± 0.12 and 0.63 ± 0.11 μm min^{-1} atm^{-1}) (Table 2) and the value for E_a of the L_p was high (12.3 and 11.6 kcal/mol) (Table 2), in which case water is expected to permeate through the plasma membrane predominately by simple diffusion [10]. In morulae, on the other hand, the average value for L_p at 25°C was quite high (4.45 ± 1.83 μm min^{-1} atm^{-1}), although the L_p value varied quite widely among embryos, from 2.04 to 9.35 μm min^{-1} atm^{-1} (data not shown). The value for E_a of the L_p was quite low (6.3 kcal/mol) (Table 2), in which case water is expected to move predominately through water channels [10]. In early blastocysts, L_p was also high (3.61 ± 1.72 μm min^{-1} atm^{-1}) and the value for E_a of the L_p was also quite low (5.1 kcal/mol) (Table 2). These results strongly suggest that most water molecules move across the
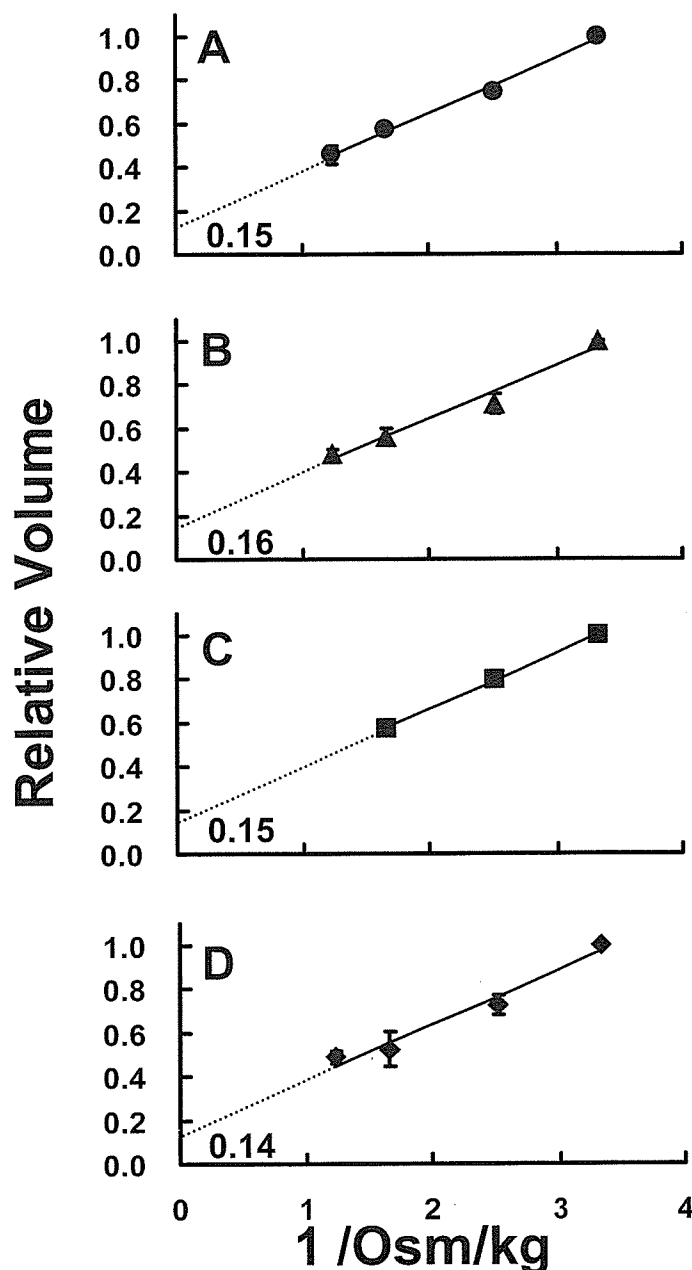

FIG. 1. Boyle-van't Hoff plots of mouse oocytes (A) and embryos at the four-cell (B), morula (C), and early blastocyst (D) stages. Oocytes (n = 5) and embryos at the four-cell (n = 5), morula (n = 4), and early blastocyst (n = 5) stages were exposed to various concentrations of sucrose in PB1 medium (0.405, 0.605, and 0.800 Osm/kg) at 25°C for 60 min, and relative volumes at 60 min were measured. Data are indicated as means of relative volume ± SD.

plasma membrane by simple diffusion in oocytes and four-cell embryos but by facilitated diffusion through water channels in morulae and early blastocysts.

Effects of Water-Channel Inhibitors on Water Permeability of Oocytes and Morulae

To examine whether water permeates through water channels, we also examined the effect of water-channel inhibitors on the L_p of oocytes and morulae. As shown in Figure 3, neither phloretin nor p-CMBS affected the L_p of oocytes, whereas both inhibitors suppressed the L_p of morulae;
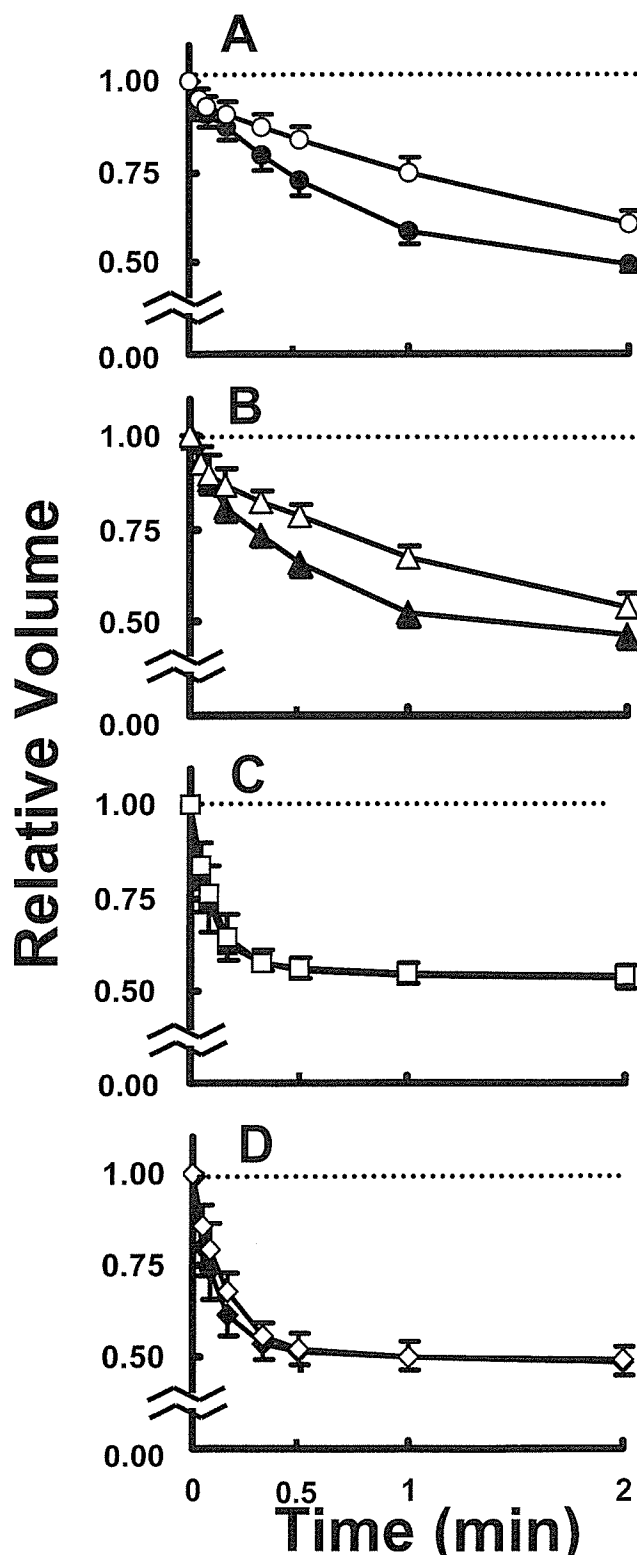
FIG. 2. Change in volume of mouse oocytes (A) and embryos at the four-cell (B), morula (C), and early blastocyst (D) stages in a hypertonic sucrose solution at 15°C (open symbols) and 25°C (closed symbols). Oocytes and embryos were exposed to sucrose in PB1 medium (0.800 Osm/kg) at 15 or 25°C for 5 min. Graphs show the volume changes during the first 2 min. Data are indicated as means of relative volume ± SD. Curves of oocytes and embryos at the four-cell, morula, and early blastocyst stages at 15°C are from 20 oocytes and 13, 26, and 22 embryos, respectively, and those at 25°C are from 27 oocytes and 17, 13, and 26 embryos, respectively.

TABLE 2. Hydraulic conductivity (L_p) and Arrhenius activation energy (E_a) of mouse oocytes and embryos.[a]

Oocytes/Embryos	L_p $(\mu m\ min^{-1}atm^{-1})$[b]		E_a (kcal/mol)
	15°C	25°C	
Oocyte	0.34 ± 0.07	0.70 ± 0.12[c]	12.3
4-cell embryo	0.32 ± 0.08	0.63 ± 0.11[c]	11.6
Morula	3.07 ± 1.39	4.45 ± 1.83[d]	6.3
Blastocyst	2.68 ± 0.98	3.61 ± 1.72[d]	5.1

[a] Values are calculated from data in Figure 2.
[b] Values are expressed as means ± SD.
[c,d] Values with different superscripts within the same column are significantly different (Student t-test; $P < 0.01$).

treatment with phloretin and p-CMBS reduced the L_p value of morulae significantly from 4.24 ± 1.76 to 2.42 ± 0.94 µm min^{-1} atm^{-1} and from 3.31 ± 0.88 to 1.94 ± 0.75 µm min^{-1} atm^{-1}, respectively (Table 3). These results strongly suggest that phloretin- and p-CMBS-sensitive water channels are abundantly expressed in morulae and contribute to the permeation of water.

Immunofluorescence Staining of AQP3 and AQP7 in Oocytes and Morulae

Among mRNAs of the Aqp family, those of Aqp3 and Aqp7 have been detected in morulae in ICR mice [6]. So, it is plausible that AQP3 and/or AQP7 are abundantly expressed in morulae and that water permeates through these AQPs. Thus, we examined the expression of AQP3 and AQP7 in oocytes and morulae by an immunofluorescence technique (Fig. 4). The anti-AQP antibodies did not detect AQP3 and AQP7 in oocytes but detected the marked expression of AQP3 in morulae.

These results strongly suggest that rapid water movement in morulae relies on AQP3.

Glycerol Permeability of Oocytes and Embryos

Because AQP3 transports not only water but also glycerol [24], it is plausible that mouse morulae are highly permeable to glycerol. In glycerol/PB1 at 25°C, oocytes and four-cell embryos shrank relatively slowly and reached their minimal volume (35–42% of their isotonic volume) within 30 sec (Fig. 5), but regained a little of their volume after 20 min of exposure. On the other hand, morulae and early blastocysts shrank rapidly to 64% of their isotonic volume and then regained their volume after 3 min of exposure. The values for P_{GLY} of oocytes and four-cell embryos were low (0.01 ± 0.00 and 0.06 ± 0.01 × 10^{-3} cm/min, respectively), whereas the values of morulae and early blastocysts were remarkably high (4.63 ± 0.94 and 4.10 ± 0.73 × 10^{-3} cm/min, respectively), as in the case of L_p (Table 2).

These results support the hypothesis that AQP3 plays an important role in rapid water movement in morulae and suggest that AQP3 is also involved in rapid glycerol movement in morulae. The results also suggest that channels like AQP3 are involved in glycerol movement in blastocysts.

Arrhenius Activation Energy for Glycerol Permeability of Oocytes and Morulae

To elucidate the involvement of a channel process in glycerol movement in morulae, we examined the E_a for the P_{GLY} of oocytes and morulae. At 15°C, oocytes shrank and regained their volumes markedly more slowly than at 25°C, and they regained their volumes only slightly even after 180

TABLE 3. Hydraulic conductivity (L_p) of mouse oocytes and morulae treated with water-channel inhibitors.[a]

Inhibitors	L_p (μm min^{-1}atm^{-1})[b]	
	Before treatment	After treatment
Oocyte		
Control	0.67 ± 0.14	0.63 ± 0.17
Phloretin	0.77 ± 0.15	0.86 ± 0.20
p-CMBS	0.70 ± 0.16	0.71 ± 0.16
Morula		
Control	3.28 ± 1.32	3.06 ± 0.90
Phloretin	4.24 ± 1.76	$2.42 \pm 0.94*$
p-CMBS	3.31 ± 0.88	$1.94 \pm 0.75*$

[a] Values for control are calculated from 10 oocytes and 10 morulae, and other values are calculated from the data in Figure 3.
[b] Values are expressed as means $\pm$ SD.
* Significantly different from the L_p before treatment (Student t-test; $P < 0.01$).

min of exposure (Fig. 6A). On the other hand, morulae shrank and regained their original volumes only after 5 min of exposure at 15°C (Fig. 6B). The value of E_a for the P_{GLY} of oocytes was quite high (41.6 kcal/mol), whereas that of morulae was relatively low (10.0 kcal/mol) (Table 4), suggesting that glycerol permeates into oocytes mainly by simple diffusion whereas it permeates into morulae by facilitated diffusion through the plasma membrane.

Effects of Water-Channel Inhibitors on Glycerol Permeability of Morulae

To examine whether glycerol permeates through water channels in morulae, we examined the effect of water-channel inhibitors on P_{GLY} of morulae. As shown in Figure 7 and Table 5, both inhibitors suppressed the permeability of morulae; pretreatment with phloretin and p-CMBS reduced the P_{GLY} value of morulae significantly from 5.17 ± 1.56 to $3.15 \pm 1.19 \times 10^{-3}$ cm/min and from 5.11 ± 0.80 to $2.92 \pm 1.13 \times 10^{-3}$ cm/min, respectively (Table 5). In control morulae, no difference was observed between the P_{GLY} values of first exposure and second exposure to glycerol/PB1.

These results suggest that phloretin- and p-CMBS-sensitive water channels and/or glycerol channels are abundantly expressed in mouse morulae and that the channels contribute to the permeation of the embryos by glycerol.

DISCUSSION

In this study, we show that the movement of water in mouse embryos at the morula stage relies on channel processes and suggest that the movement of glycerol in morulae also relies on channel processes.

TABLE 4. Glycerol permeability (P_{GLY}) at 15 and 25°C and Arrhenius activation energy (E_a) of mouse oocytes and morulae.[a]

Oocyte/Embryo	P_{GLY} ($\times 10^{-3}$ cm/min)[b]		E_a (kcal/mol)
	15°C	25°C	
Oocyte	0.00 ± 0.00	0.02 ± 0.02^c	41.6
Morula	2.61 ± 0.88	4.68 ± 1.50^d	10.0

[a] Values are calculated from the data in Figure 6.
[b] Values are expressed as means $\pm$ SD.
[c,d] Values with different superscripts within the same column are significantly different (Student t-test; $P < 0.01$).
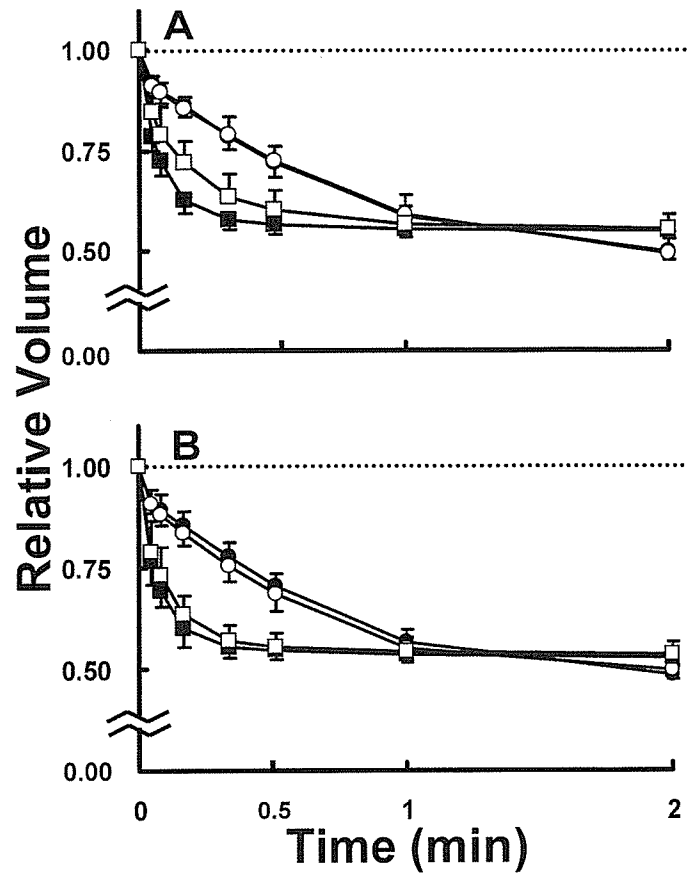

FIG. 3. Inhibition of water permeability of mouse oocytes and morulae by water-channel inhibitors. Oocytes (circles) and morulae (squares) were exposed to 0.7 mM phloretin in PB1 medium at 25°C for 2.5 min (A) (n = 10 and n = 10, respectively) or 0.5 mM p-(chloromercuri) benzene-sulfonate in PB1 medium at 25°C for 30 min (B) (n = 12 and n = 11, respectively). Hydraulic conductivity was calculated from volume changes of oocytes and morulae in sucrose in PB1 medium (0.800 Osm/kg) at 25°C for 5 min before (closed symbols) and after (shaded symbols) treatment with the inhibitor. Graphs show the volume changes during the first 2 min. Data are indicated as means of relative volume $\pm$ SD. In A, the untreated and treated oocyte data points fall on top of each other.

Mature oocytes had low L_p and high E_a values (0.70 μm min^{-1} atm^{-1} and 12.3 kcal/mol, respectively) (Table 2). These values are similar to those of other studies [11–17] and suggestive of water movement by simple diffusion across the plasma membrane [10]. Four-cell embryos also had low L_p and high E_a values (0.63 μm min^{-1} atm^{-1} and 11.6 kcal/mol, respectively), similar to those of oocytes (Table 2). This L_p value is similar to that reported in another study (0.73 μm min^{-1} atm^{-1}) [16]. Thus, it appears that water also permeates through the plasma membrane of four-cell embryos primarily by simple diffusion.

On the other hand, morulae and early blastocysts had very high L_p and very low E_a values (4.45 and 3.61 μm min^{-1} atm^{-1} and 6.3 and 5.1 kcal/mol, respectively) (Table 2). The L_p value is close to 4.5 μm min^{-1} atm^{-1} and the E_a value is also close to 6 kcal/mol, suggesting the dependence of water movement on a channel pathway [10]. Thus, most water molecules would move across the plasma membrane through channel processes in morulae and blastocysts. Moreover, values for the L_p of morulae varied quite widely from 2.04 to 9.35 μm min^{-1} atm^{-1} among embryos (data not shown). The high variation in L_p can be explained by the different levels of channel expression
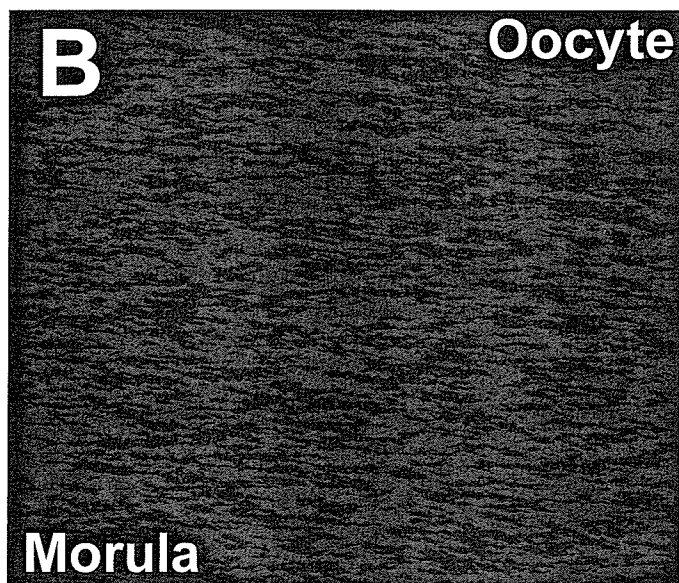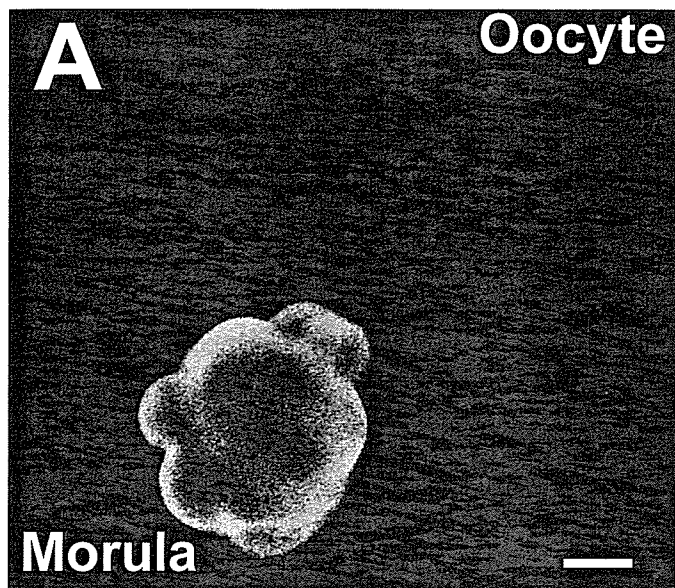
FIG. 4. Expression of aquaporin 3 (A) and aquaporin 7 (B) in a mouse oocyte and a morula. Expression of aquaporin proteins was detected by an immunofluorescence technique with anti-aquaporin 3 antibody (A) or anti-aquaporin 7 antiserum (B). Bar = 20 μm.

among morulae but not by simple diffusion across the plasma membrane. Furthermore, AQP inhibitors did not affect the L_p of oocytes but significantly suppressed that of morulae (Table 3). All of these results strongly suggest that water channels are the major contributor to water movement in morulae and early blastocysts.

There has been no report that suggests that experimentally water-permeable channels other than AQPs expressed in the plasma membrane at physiological levels contribute to total plasma membrane water permeability [26]. Thus, AQPs may be the major contributor to the permeation of mouse morulae and early blastocysts by water.

We have already shown that mRNAs of $Aqp3$ and $Aqp7$ are present in mouse oocytes at the metaphase II stage and embryos from the four-cell to morula stages but those of other Aqps were not in ICR mice [6]. Thus, these two AQPs may be
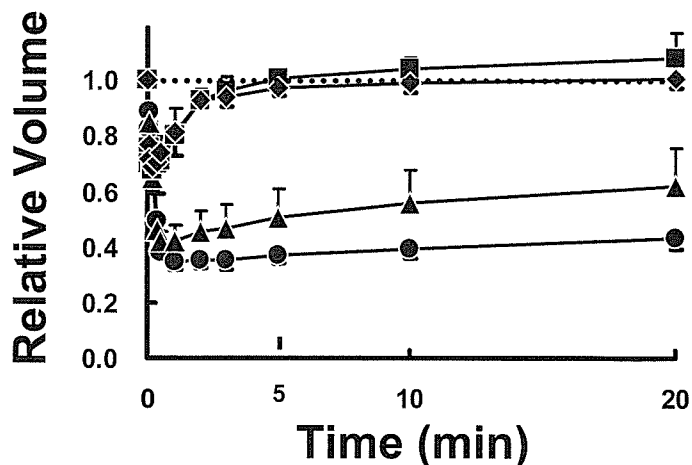

FIG. 5. Change in volume of mouse oocytes and embryos in 10% glycerol solution at 25°C. Mouse oocytes (circles) (n = 18) and embryos at the four-cell (triangles) (n = 7), morula (squares) (n = 14), and early blastocyst (diamonds) (n = 8) stages were exposed to 10% (vol/vol) glycerol in PB1 medium at 25°C for 20 min. Data are indicated as means of relative volume ± SD.

involved in the marked increase in the L_p of the embryos at the morula stage. Offenberg et al. [7] and Offenberg and Thomsen [8] reported the expression of mRNAs of other Aqps, including $Aqp1$, $Aqp5$, and $Aqp6$, in CD-1 X CB6F1/J embryos at various stages. The reason for this discrepancy is not known, but there may be mouse strain-specific differences in Aqp mRNA subtypes present.

It is known that mercuric compounds, such as $HgCl_2$ and p-CMBS, inhibit various AQPs, including AQP1, AQP2, and AQP3, by binding to a critical sulfhydryl [27], but not AQP7 because it does not have a critical sulfhydryl [25]. Phloretin is known as a urea-transporter inhibitor and inhibits the transport of water by AQP3 [24, 28], although its effect on AQP7 is not known. Thus, it was expected that phloretin and p-CMBS would decrease the L_p of morulae if AQP3 was dominantly expressed in morulae, whereas the inhibitors might not affect the L_p if AQP7 was dominantly expressed. Both phloretin and p-CMBS significantly reduced the L_p of morulae (Fig. 3 and Table 3), supporting the former assumption that AQP3 was expressed dominantly in morulae.

This hypothesis was confirmed by detection of the marked expression of AQP3 protein on the apical side of blastomeres of morulae but not in oocytes by an immunofluorescence technique (Fig. 4A). On the other hand, little expression of AQP7 was detected in oocytes or morulae (Fig. 4B). Thus, AQP3 must be the major contributor to water transport in morulae.

TABLE 5. Glycerol permeability (P_{GLY}) of mouse morulae treated with water-channel inhibitors.[a]

Inhibitors	P_{GLY} ($\times 10^{-3}$ cm/min)[b]	
	Before treatment	After treatment
Control	4.62 ± 0.92	4.72 ± 0.83
Phloretin	5.17 ± 1.56	3.15 ± 1.19*
p-CMBS	5.11 ± 0.80	2.92 ± 1.13*

[a] Values for control are calculated from 10 morulae, and other values are calculated from the data in Figure 7.
[b] Values are expressed as means ± SD.
* Significantly different from the P_{GLY} before treatment (Student t-test; $P <$ 0.01).
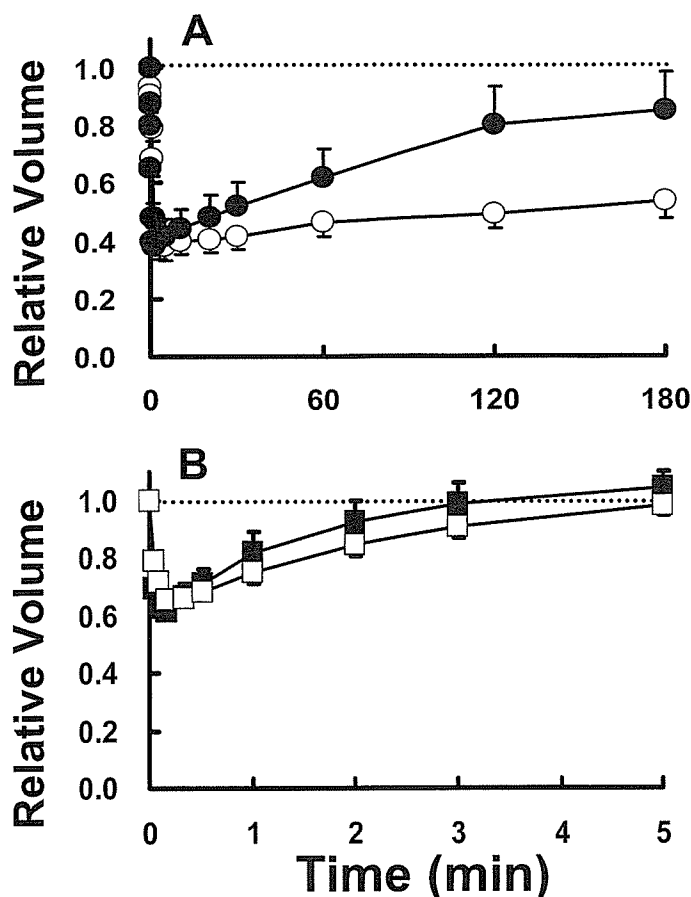
FIG. 6. Change in volume of mouse oocytes (A) and morulae (B) in 10% glycerol solution at 15°C (open symbols) and 25°C (closed symbols). Oocytes were exposed to 10% (vol/vol) glycerol in PB1 medium (1.89 Osm/kg) at 15 and 25°C for 180 min, and morulae were exposed to the solutions for 5 min. Data are indicated as means of relative volume ± SD. Each curve is from six oocytes or six morulae.

FIG. 7. Inhibition of glycerol permeability of mouse morulae by water-channel inhibitors. Morulae were exposed to 0.7 mM phloretin (A) or 0.5 mM p-(chloromercuri) benzensulfonate (B) in PB1 medium. Glycerol permeability was calculated from volume changes of morulae in 10% (vol/vol) glycerol in PB1 medium at 25°C for 5 min before (closed symbols) and after (shaded symbols) treatment with the inhibitor. Data are indicated as means of relative volume ± SD. Each curve is from 10 oocytes or 10 morulae.

Barcroft et al. [9] also reported that AQP3 was detected markedly on the apical side of blastomeres of morulae of CD-1 X CB6F1/J mice. Moreover, they did not detect other AQPs on the apical side of blastomeres of the morulae, although they detected other AQPs in the region of cell-cell contact. Thus, in morulae, the major water pathway must be AQP3 in the mouse.

In early blastocysts, the additional expression of mRNAs of *Aqp8* and *Aqp9*, in addition to those of *Aqp3* and *Aqp7*, has also been observed in ICR mice [6]. Barcroft et al. [9] showed in CD-1 X CB6F1/J embryos that expression of AQP3 became restricted in the inner cell mass and the basolateral cell margins of the trophectoderm and that AQP9 was expressed in the inner cell mass and the apical membrane of the trophectoderm. If the AQPs are distributed in blastocysts of ICR mice similarly, AQPs other than AQP3 could play a role in water movement in the blastocysts. Because the blastocysts we used were pipetted repeatedly to shrink their blastocoele and thus may have had small rips in their trophectoderm from the pipetting, it is possible that water moved not only across the apical side but also across the blastocoele-side of the plasma membrane in hypertonic sucrose solution. Thus, AQPs expressed in the inner cell mass and the basolateral cell margins of the trophectoderm might partially contribute to the water movement in our experiments. Further studies are needed to clarify which type of AQP is involved in water movement in mouse blastocysts.

AQP3 is an aqua glyceroporin, which can transport not only water but also neutral solutes with a low molecular weight,
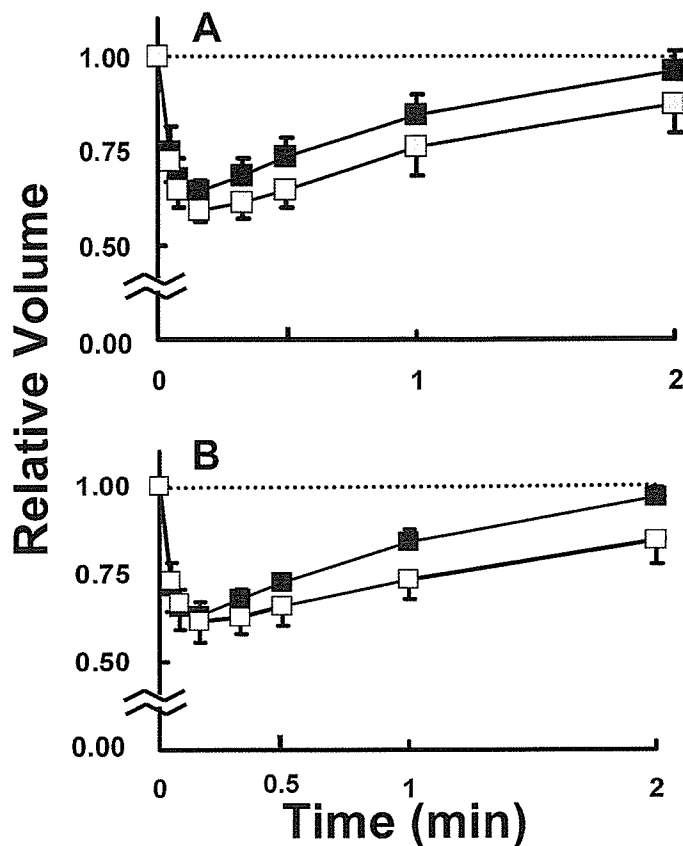
such as glycerol [24]. Thus, we examined the P_{GLY} of mouse oocytes and embryos (Fig. 5). The P_{GLY} of oocytes and four-cell embryos was low (0.01–0.06 × 10^{-3} cm/min), whereas that of morulae was high (4.63 × 10^{-3} cm/min), being more than 100 times higher than that of oocytes. This result suggests that AQP3 plays a role in the marked increase in the permeability of morulae to glycerol.

The pioneering studies by Mazur and his group [29, 30] demonstrated that the permeability of mouse embryos to glycerol increased from oocytes and one-cell zygotes to eight-cell embryos. The P_{GLY} values of oocytes and four-cell embryos in their studies (0.01 and 0.05 × 10^{-3} cm/min, respectively, at 20–22°C) are almost the same as those in the present study (0.01 and 0.06 × 10^{-3} cm/min, respectively, at 25°C). They also reported that a marked increase in the P_{GLY} of embryos was observed at the eight-cell stage (0.34 × 10^{-3} cm/min). In the present study, we observed further remarkable increase in the P_{GLY} at the morula stage (4.63 × 10^{-3} cm/min at 25°C). Thus, the marked increase in the expression of glycerol-permeable channels appears to begin at around the stage when mouse embryos develop to compacted morulae.

Thus, we studied the E_a for P_{GLY} and the sensitivity of P_{GLY} to AQP inhibitors in oocytes and morulae. The value of E_a for the P_{GLY} of oocytes was quite high (41.6 kcal/mol), whereas that of morulae was much lower (10.0 kcal/mol) (Table 4). The marked decrease in E_a suggests that channel processes play a role in rapid glycerol movement in morulae. Moreover,

phloretin and p-CMBS suppressed the P_{GLY} of morulae significantly (Table 5), suggesting that channels sensitive to these inhibitors were involved in glycerol movement in morulae. It has been shown that p-CMBS also suppresses the P_{GLY} of AQP3 [24, 28]. On the other hand, phloretin suppresses the L_p [24, 28] but not P_{GLY} of AQP3 [28]. Thus, rapid glycerol movement in morulae should rely partly on AQP3, but other glycerol channels might be involved in the process.

Early blastocysts also had remarkably high glycerol permeability, like the morulae (Fig. 5), suggesting that glycerol movement in blastocysts also relies on channel processes. It has been reported that the permeation by glycerol into CD-1 X CB6F1/J blastocysts is suppressed by p-CMBS [9]. Thus, mouse blastocysts also have mercury-sensitive channel-dependent glycerol pathways, the same as morulae. Further studies are needed to clarify which channels are involved in glycerol transport in blastocysts.

We have already examined changes in volume of mouse oocytes and embryos in various cryoprotectant solutions in preliminary experiments and showed that the pattern of cryoprotectant permeation does not change from matured oocytes up to embryos at the two-cell stage, but permeability to glycerol and ethylene glycol drastically increases at around the morula stage [20]. In bovine oocytes and embryos, we have also observed similar changes; the pattern of cryoprotectant permeation does not change from matured oocytes up to embryos at the 16-cell stage, but permeability to ethylene glycol and glycerol drastically increases at the morula stage [31]. Thus, the marked increase in aqua glyceroporins, such as AQP3, in the later stages of development may occur not only in the mouse but also in other mammalian species. Such increased permeability of mammalian embryos might play a role in the uptake of small molecules from tubal or uterine fluid or in the excretion of metabolites from embryos. However, the role appears not to be vital for the development of mouse embryos because *Aqp3* knockout mice can develop to term and are grossly normal except for polyurea [32]. However, because aqua glyceroporins are permeable to various cryoprotectants, the expression may also affect the tolerance of embryos at different developmental stages to cryopreservation. Thus, the present study provides important information for understanding the cryobiological properties of mammalian oocytes and embryos and for formulating cryopreservation protocols for mammalian oocytes and embryos.

REFERENCES

1. Whittingham DG, Leibo SP, Mazur P. Survival of mouse embryos frozen to −196°C and −269°C. Science 1972; 178:411–414.
2. Kasai M, Komi JH, Takakamo A, Tsudera H, Sakurai T, Machida T. A simple method for mouse embryo cryopreservation in a low toxicity vitrification solution, without appreciable loss of viability. J Reprod Fertil 1990; 89:91–97.
3. Kasai M. Cryopreservation of mammalian embryos. Mol Biotech 1997; 7:173–179.
4. Kasai M, Ito K, Edashige K. Morphological appearance of the cryopreserved mouse blastocyst as a tool to identify the type of cryoinjury. Hum Reprod 2002; 17:1863–1874.
5. King LS, Kozono D, Agre P. From structure to disease: the evolving tale of aquaporin biology. Nat Rev Mol Cell Biol 2004; 5:687–698.
6. Edashige K, Sakamoto M, Kasai M. Expression of mRNAs of the aquaporin family in mouse oocytes and embryos. Cryobiology 2000; 40:171–175.
7. Offenberg H, Barcroft LC, Caveney A, Viuff D, Thomsen PD, Watson AJ. mRNAs encoding aquaporins1–9 are present during murine preimplantation development. Mol Reprod Dev 2000; 57:1–8.
8. Offenberg H, Thomsen PD. Functional challenge affects aquaporin mRNA abundance in mouse blastocysts. Mol Reprod Dev 2005; 71:422–430.
9. Barcroft LC, Offenberg H, Thomsen P, Watson AJ. Aquaporin proteins in murine trophectoderm mediate transepithelial water movements during cavitation. Dev Biol 2003; 256:342–354.
10. Verkman AS, van Hoek AN, Ma T, Frigeri A, Skach WR, Mitra A, Tamarappoo BK, Farinas J. Water transport across mammalian cell membranes. Am J Physiol 1996; 270:C12–30.
11. Leibo SP. Water permeability and its activation energy of fertilized and unfertilized mouse ova. J Membrane Biol 1980; 53:179–188.
12. Hunter J, Bernard A, Fuller B, McGrath J, Shaw RW. Measurements of the membrane water permeability (L_p) and its temperature dependence (activation energy) in human fresh and failed-to-fertilize oocytes and mouse oocytes. Cryobiology 1992; 29:240–249.
13. Benson CT, Critser JK. Variation of water permeability (L_p) and its activation energy (E_a) among unfertilized golden hamster and ICR murine oocytes. Cryobiology 1994; 31:215–223.
14. Gao DY, Benson CT, Liu C, McGrath JJ, Critser ES, Critser JK. Development of novel microperfusion chamber for determination of cell membrane transport properties. Biophys J 1996; 71:443–450.
15. Litkouhi B, Marlow D, McGrath JJ, Fuller B. The influence of cryopreservation on murine oocyte water permeability and osmotically inactive volume. Cryobiology 1997; 34:23–35.
16. Pfaff RT, Liu J, Gao D, Peter AT, Li TK, Critser JK. Water and DMSO membrane permeability characteristics of in-vivo and in-vitro derived and cultured murine oocytes and embryos. Mol Hum Reprod 1998; 4:51–59.
17. Toner M, Cravalho EG, Armant DR. Water transport and estimated transmembrane potential during freezing of mouse oocytes. J Membrane Biol 1990; 115:261–272.
18. Pedro PB, Zhu SE, Makino N, Sakurai T, Edashige K, Kasai M. Effects of hypotonic stress on the survival of mouse oocytes and embryos at various stages. Cryobiology 1997; 35:150–158.
19. Edashige K, Yamaji Y, Kleinhans FW, Kasai M. Artificial expression of aquaporin-3 improves the survival of mouse oocytes after cryopreservation. Biol Reprod 2003; 68:87–94.
20. Pedro PB, Yokoyama E, Zhu SE, Yoshida N, Valdez DM Jr, Tanaka M, Edashige K, Kasai M. Permeability of mouse oocytes and embryos at various developmental stages to five cryoprotectants. J Reprod Dev 2005; 51:235–246.
21. Kleinhans FW. Membrane permeability modeling: Kedem-Katchalsky vs a two-parameter formalism. Cryobiology 1998; 37:271–289.
22. Wolf AV, Brown MG, Prentiss PG. Concentration properties of aqueous solutions: conversion tables. In: Weast RC, (ed.), Handbook of Chemistry and Physics, 51st ed. Cleveland: Chemical Rubber Co.; 1970:D181–D226.
23. Hogan B, Beddington R, Costantini F, Lacy E. Removing the zona pellucida. In: Hogan B, Beddington R, Costantini F, Lacy E (eds.), Manipulating the Mouse Embryo, 2nd ed. New York: Cold Spring Harbor Laboratory Press; 1994:191.
24. Ishibashi K, Sasaki S, Fushimi K, Uchida S, Kuwahara M, Saito H, Furukawa T, Nakajima K, Yamaguchi Y, Gojobori T, Marumo F. Molecular cloning and expression of a member of the aquaporin family with permeability to glycerol and urea in addition to water expressed at the basolateral membrane of kidney collecting duct cells. Proc Natl Acad Sci U S A 1994; 91:6269–6273.
25. Ishibashi K, Kuwahara M, Gu Y, Kageyama Y, Tohsaka A, Suzuki F, Marumo F, Sasaki S. Cloning and functional expression of a new water channel abundantly expressed in the testis permeable to water, glycerol, and urea. J Biol Chem 1997; 272:20782–20786.
26. Verkman AS, Mitra AK. Structure and function of aquaporin water channels. Am J Physiol Renal Physiol 2000; 278:F13–F28.
27. Preston GM, Jung JS, Guggino WB, Agre P. The mercury-sensitive residue at cysteine 189 in the CHIP28 water channel. J Biol Chem 1993; 268:17–20.
28. Tsukaguchi H, Shayakul C, Berger UV, Mackenzie B, Devidas S, Guggino WB, van Hoek AN, Hediger MA. Molecular characterization of a broad selectivity neutral solute channel. J Biol Chem 1998; 273:24737–24743.
29. Mazur P, Rigopoulos N, Jackowski SC, Leibo SP. Preliminary estimates of the permeability of mouse ova and early embryos to glycerol. Biophys J 1976; 16:232a.
30. Jackowski S, Leibo SP, Mazur P. Glycerol permeability of fertilized and unfertilized mouse ova. J Exp Zool 1980; 212:329–341.
31. Pedro PB, Kasai M, Mammaru Y, Yokoyama E, Edashige K. Change in the permeability to different cryoprotectants of bovine oocytes and embryos during maturation and development. Proc 13th Int Congr Anim Reprod 1996; 3:15–9.
32. Ma T, Song Y, Yang B, Gillespie A, Carlson EJ, Epstein CJ, Verkman AS. Nephrogenic diabetes insipidus in mice lacking aquaporin-3 water channels. Proc Natl Acad Sci U S A 2000; 97:4386–4391.

ELSEVIER

CRYOBIOLOGY

Extra- and intra-cellular ice formation in Stage I and II Xenopus laevis oocytes ☆

James F. Guenther [a], Shinsuke Seki [a,b], F.W. Kleinhans [a,1], Keisuke Edashige [a,b], Daniel M. Roberts [c], Peter Mazur [a,*]

[a] Fundamental and Applied Cryobiology Group, Department of Biochemistry and Cellular and Molecular Biology, The University of Tennessee, Knoxville, TN 37932-2575, USA
[b] Laboratory of Animal Science, College of Agriculture, Kochi University, Kochi, Japan
[c] Department of Biochemistry and Cellular and Molecular Biology, The University of Tennessee, Knoxville, TN 37932-0840, USA

Abstract

We are currently investigating factors that influence intracellular ice formation (IIF) in mouse oocytes and oocytes of the frog Xenopus. A major reason for choosing these two species is that while their eggs normally do not possess aquaporin channels in their plasma membranes, these channels can be made to express. We wish to see whether IIF is affected by the presence of these channels. The present Xenopus study deals with control eggs not expressing aquaporins. The main factor studied has been the effect of a cryoprotective agent [ethylene glycol (EG) or glycerol] and its concentration. The general procedure was to (a) cool the oocytes on a cryostage to slightly below the temperatures at which extracellular ice formation occurs, (b) warm them to just below the melting point, and (c) then re-cool them to -50 °C at 10 °C/min. In the majority of cases, IIF occurs well into step (c), but a sizeable minority undergo IIF in steps (a) or (b). The former group we refer to as low-temperature flashers; the latter as high-temperature flashers. IIF is manifested as abrupt blackening of the egg, which we refer to as "flashing." Observations on the Linkam cryostage are restricted to Stage I and II oocytes, which have diameters of 200–300 μm. In the absence of a cryoprotective agent, that is in frog Ringers, the mean flash temperature for the low-temperature freezers is -11.4 °C, although a sizeable percentage flash at temperatures much closer to that of the EIF (-3.9 °C). When EG is present, the flash temperature for the low-temperatures freezers drops significantly to ~ -20 °C for EG concentrations ranging from 0.5 to 1.5 M. The presence of 1.5 M glycerol also substantially reduces the IIF temperature of the low-temperature freezers; namely, to -29 °C, but 0.5 and 1 M glycerol exert little or no effect. The IIF temperatures observed using the Linkam cryostage agree well with those estimated by calorimetry [F.W. Kleinhans, J.F. Guenther, D.M. Roberts, P. Mazur, Analysis of intracellular ice nucleation in Xenopus oocytes by differential scanning calorimetry, Cryobiology 52 (2006) 128–138]. The IIF temperatures in Xenopus are substantially higher than those observed in mouse oocytes [P. Mazur, S. Seki, I.L. Pinn, F.W. Kleinhans, K. Edashige,